Nitrogen and boron doping in carbon nanotubes

Chris Ewels
Institute des Materiaux, UMR6502 CNRS-Université de Nantes, 2 rue de la Houssinière, B. P. 32229, 44322 Nantes, France.

Mail: chris@ewels.info*, Tel:+33 2 40 37 64 07, Fax: +33 2 40 37 39 91, Web: www.ewels.info*

Marianne Glerup
Department of Chemistry, University of Oslo, PO Box 1033, 0315 Oslo, Norway.

Mail: marianne.glerup@kjemi.uio.no, Tel*:+47 228 55676 Fax: +47 228 55441*

Vojislav Krstić
National Pulsed Magnetic Field Laboratory (LNCMP), 143 Avenue de Rangueil, 31400 Toulouse, France.

Mail: Krstić@lncmp.org, Tel: +33 5 62 17 28 19, Fax: +33 5 62 17 28 16

To appear in "Chemistry of Carbon Nanotubes", edited by V. A. Basiuk and E. V. Basiuk (to be published, 2007), American Scientific Publishers.

CONTENTS

1.1 Introduction

Although the properties of carbon nanotubes are nothing short of exceptional, there are nonetheless many areas in nano- and molecular-electronics, optics, electro-mechanics or chemistry where pristine tubes are not the most appropriate. This is because of their rather wide spread characteristic physical and chemical properties, which is a result of the diameter and helicity variations of a nanotube samples.
Substitutional doping of nanotubes is expected to provide solutions for these limitations. Indeed, the incorporation of boron and nitrogen atoms into the honeycomb lattice leads to chemical activation of the rather passive surface of a carbon nanotube and adds additional electronic states around the Fermi level.

It has to be stressed that the characterisation of the effects doping has on a single nanotube is difficult to qualitatively and quantitatively determine. These problems arise mainly because of sample impurities; dopant concentrations; single tube measurements. The characterisation comprises the direct probing of the dopants in the nanotube and the overall effect the dopants has on the nanotube properties.

To date, nitrogen doping concentrations in SWNTs are limited to around 1% [1], whereas in MWNTs average concentrations can reach ~15-20 at% [2] with local concentrations up to 25-30% [3]. A dark-field image of nitrogen doped nanotubes is given in Figure 1.

Nitrogen doping of tubes has received considerable attention in the area of nanoelectronics, as a direct analogue of conventional heteroatom doping in bulk semiconductors. Next generation nanoelectronics based on nanotubes will require *n*-

and *p*- doping for diode and transistor construction, indeed, the tantalising possibility of spatially located doping raises the possibility of whole device construction within a single nanotube.

Extrinsic doping of nanotube surfaces can lead to localised electronic states. This disrupts the smooth, largely chemically inert, nanotube π-cloud, making the tubes chemically active. For this reason extrinsically doped tubes should make excellent starting candidates for a new generation of controlled chemically functionalised nanotube materials. In the case of non-homogenously distributed dopants within the tube wall, doping provides a way to 'activate' regions along the tube wall. For single-walled nanotubes (SWNTs), and for the outer layer of multi-walled nanotubes (MWNTs), this will lead to increased surface reactivity. These regions can be utilised for chemical functionalisation with molecules and maybe also for tube-tube fusion and junction formation. Notably many applications require chemical functionalisation or chemically active nanotube surfaces, those requiring solubility of the nanotubes, and those needing high electron densities near the Fermi level.

Nitrogen doped tubes are also under active investigation for use in field emission, Li-ion storage, as gas sensors, in polymer-CNT composites, amongst other areas. One property that may yet prove the most important for nitrogen doped tubes is biocompatibility. Nanotubes functionalised to render them water soluble were directly expelled from test rats in their urine [4], whereas studies of pristine nanotubes appear to suggest absorption and retention in the body (notably within the organs) over much longer time scales [5]. Toxicological studies of nitrogen doped nanotubes in rats showed significantly lower toxic response than for their pristine MWNT counterparts

[6]; it thus appears that the chemical activation of nanotube surfaces caused by nitrogen doping, and possible presence of amide surface renders them more biocompatible than their pristine counterparts. There is a huge interest in the use of carbon nanotubes in biology, and substitutional doped tubes may prove to be the material of choice for these applications.

It is important to note that the doping regimes required for different applications are vastly different. Impurity doping in classical semiconductors is at low concentrations (typically at concentrations of 10^{-9} at%), below the detection limit for many of the spectroscopic techniques discussed below. Low concentration doping will require very different growth regimes and sample treatment from those needed, for example, aimed at growing mixed- stoichiometry C_3N_4 tubular materials.

One of the attractive properties of carbon nanotubes (especially SWNTs) is that the material is effectively all surface. This opens up the possibility of doping techniques not available in conventional three-dimensional materials, notably chemical functionalisation of the tube surface, π-stacking with aromatic or aromatic-containing molecules, tube wrapping with electropositive or electronegative polymers, tube coating with metal ions [7, 8], and even surface coating with nanoscopic layers of inorganic material. For to good reviews on this topic see Refs. [9][10]. A complete review of all these techniques is beyond the scope of the current work, and we instead constrain ourselves to considering only nitrogen doping through insertion into the carbon nanotube walls. Also beyond the scope of this chapter is the range of BN and BC_xN_y nanotubes now being grown in both single and multi-walled forms, a new and interesting range of materials with excellent mechanical properties and the potential

for tuneable electronic band gaps. There has been much work on N_2 physisorption on carbon nanotubes, see for example Refs. [11], but since this does not involve nitrogen insertion into the nanotube lattice it will not be covered here.

This chapter is structured as follows. We first provide an introduction to the field of nitrogen doped carbon nanotubes (N-CNTs) and a brief overview of their properties. There then follows N-CNT synthesis techniques, and the resultant doped nanotube morphology and possible growth mechanisms. Since the nitrogen doped nanotube literature relies heavily on that of the nitrogen doped carbon film research, it is instructive to consider briefly other nitrogen doped carbon materials. We therefore review possible layered CN_x phases as pointers to high nitrogen concentration structures. We next examine possible atomic configurations for nitrogen in the nanotube lattice and discuss their electronic properties. This is followed by the various spectroscopic studies of N-CNTs and theoretical attempts to assign these peaks to specific nitrogen configurations. We then discuss the role of nanotube curvature and chirality, as well as possibilities for cross-linking and defect-defect interaction. There then follows a brief review of new studies on the surface chemistry of nitrogen doped CNTs. Finally we cover electronic transport properties of N-CNTs, and possible applications, before drawing some overall conclusions and offering some future perspectives for these interesting new materials.

In this chapter we focus on nitrogen doping since it is the area that has seen the most active research interest. We therefore only discuss boron doping where it is instructive to compare with nitrogen doping.

1.2 Introduction to nitrogen doped nanotubes and their properties

Substitutional doping of carbon nanotubes was first attempted by Stéphan *et al.* [12] in 1994, they synthesising boron-nitrogen doped MWNTs using the arc-discharge method.

Nitrogen doped SWNTs generally exhibit morphologies similar to their undoped counterparts, namely straight non-buckled nanotube walls [1, 13]. However nitrogen doped MWNTs exhibit very distinct morphologies, significantly different from their undoped counterparts. These tubes always have a so-called 'bamboo' structure, where the nanotube contains a regularly spaced array of internal carbon walls, or alternatively similar 'nano-bell' structures where the tube appears to be a linearly stacked line of bell-shaped cavities. The alignment and number of nanotube walls depends on dopant concentration and catalyst used, and the walls are often more buckled and irregular than those of undoped MWNTs. Representative examples of the morphology of nitrogen-doped SWNTs and MWNTs are given in Figure 2.

Nitrogen doped nanotubes are less stable than their pure carbon counterparts, breaking easily under the electron beam in the transmission electron microscope (TEM) [1] and oxidising at lower temperatures than undoped tubes [14]. This is understandable when one considers the nitrogen atoms as localised defects, which will be energetically less stable than a pure carbon lattice. This also makes the tube surfaces chemically active,

facilitating chemical functionalisation [15]. Their active surfaces mean they can be dispersed in a range of solvents not possible with undoped tubes [16].

Scanning tunnelling spectroscopy studies of several nanotubes found only metallic behaviour with a strong donor peak just above the Fermi level [17, 18] unlike undoped tubes which exhibit a variety of metallic and semiconducting behaviour depending on their chirality.

Experiments suggest fundamental limits to nitrogen doping concentrations in CNTs. In SWNTs concentrations appear limited to around 1% at most [1], whereas in MWNTs average concentrations can reach ~15-20 at% [2], and local concentrations can reach 25-30% [3]. Combined transmission electron microscope (TEM) and electron energy loss spectroscopy (EELS) studies of nitrogen doped MWNTs only detected nitrogen in tubes with diameters over 10 nm, despite the presence of tubes down to 5 nm diameter [19].

To date the majority of experimental studies have focussed on MWNT systems, whereas theory has concentrated on doped SWNT behaviour. There are clearly many fundamental differences between these two systems, and there is plenty of scope in both sections of the community for greater overlap in this regard.

1.3 Synthesis and morphologies of nitrogen doped nanotubes

Nanotube doping can be achieved in two different ways, either directly during the synthesis or by post treatment of pre-synthesized carbon nanotubes. For both approaches various methods have successfully been employed for making nitrogen

doped carbon nanotubes. The experimental field of doped MWNTs is more advanced than that of doped SWNTs.

1.3.1 High temperature synthesis methods such as arc- discharge and laser ablation

Arc-discharge, laser ablation and the solar oven all belong to the so-called high temperature synthesis methods. The high temperature is used in all these cases to evaporate the carbon source, normally graphite [20].

The arc-discharge method was the first to be applied to doped MWNTs [21-23]. The tubes are grown through evaporation of a graphite rod *via* an electric-arc, in a helium-gas atmosphere. Another high temperature growth technique is laser ablation, whereby a catalyst containing graphite target is ablated using a pulsed laser, with the vaporisation products rapidly removed by flowing gas such as N_2. Laser ablation is also commonly used to produce nitrogen doped fullerenes (azo-fullerenes) [24-28].

A few studies have examined the possibility of doping SWNTs with nitrogen using arc-discharge. Droppa *et al* created nitrogen-doped SWNTs by the evaporation of a catalyst containing graphite rod in a nitrogen–helium atmosphere in an arc-discharge experiment [13]. They also observed that the nitrogen gave rise to an increased content of more fibrous structures. X-ray photoemission spectroscopy (XPS) was used as the main characterization technique for demonstrating successful doping. We note that in general one should take great care using bulk measurement techniques for probing hetero atoms in nanotube samples, since they reflect the average properties of

the sample which always contains a certain amount of impurities. Glerup *et al* also used an arc-discharge approach for creating hetero single-walled nanotubes [1]. They utilized composite anodes containing nitrogen rich precursors in a helium atmosphere, successfully incorporating around 1 at% nitrogen into the tubes. It was possible to directly probe the nitrogen in the nanotubes because of the dedicated EEL spectrometer used and the relatively high nitrogen concentration [12].

As far as we are aware, there have been no other high temperature synthesis techniques used such as laser ablation to create nitrogen doped SWNTs.

1.3.2 Lower temperature synthesis methods such as CVD

Nitrogen doped multi-walled nanotubes have been synthesized both by classical chemical vapor deposition techniques (CVD) and by aerosol assisted CVD methods, for a resumé see Table 1. It was for a long time assumed to be a difficult task to synthesize nitrogen doped MWNTs, and the first papers dealt with relatively low doping concentration [29, 30]. Afterwards several authors demonstrated the possibility of incorporating significant concentrations of nitrogen into multi-walled nanotubes (around 20 atom%) by aerosol assisted CVD methods [31][1],. More recently nitrogen doping in double-walled nanotubes has been demonstrated [32]. As far as we are aware there have not yet been any successful attempts to grow nitrogen doped SWNTs using CVD synthesis, although there is no reason not to expect this method to be successful.

Table 1 gives a resumé of the obtained results using these approaches and with many different catalyst precursors and carbon/nitrogen sources used. This is typically done under Ar, N_2, NH_3, or a mixture of these. Excluding the classical CVD experiments and studying only the results from the aerosol assisted- and pyrolysis- experiments a correlation between the nitrogen concentration in the nanotubes and the concentration of nitrogen in the precursor can be obtained. This correlation is not perfect but one should keep in mind that the exact experimental conditions have not been taken into account, such as temperature, choice of catalyst, and stability of the carbon and nitrogen precursors under the given reaction conditions. This shows that *in-situ* incorporation of nitrogen into MWNTs is not unfavourable. As can be seen from the table, studies to date have used a broad selection of techniques with little standardisation, making further general conclusions difficult, although systematic studies of, e.g. catalyst composition are beginning to appear [33].

It should be noted that many of the conventional undoped nanotube CVD growth techniques employ nitrogen gas as their inert gas atmosphere, e.g. laser ablation and chemical vapour deposition. It is very possible that there will be some inadvertent nitrogen incorporation in the nanotubes walls in these cases.

Solvo-thermal synthesis is another technique originally employed for synthesizing pure multi walled carbon nanotubes [34, 35], however it has now been applied to the growth of CN_x tubes. Using cyanuric chloride as a starting material in an autoclave reaction (high pressure), the authors claim to produce stable large diameter nanotubes with very high nitrogen contents [36-38].

1.3.3 Post Treatment Doping Techniques

Aside from nitrogen incorporation during growth, it is also possible to nitrogen dope nanotubes through post treatments of pristine carbon nanotubes. Chemical substitution has been used to nitrogen dope SWNTs, through partial substitution reactions of undoped tubes, using B_2O_3 vapour and N_2 gas at 1500-1700K [39]. This results in irregular damaged nanotube walls with less than 1% N substitution, comparable with arc-discharge techniques. D.C. magnetron sputtering has successfully been applied by Suenaga *et al*, achieving high nitrogen concentrations of 15-30% though mainly in the carbon nanoturbolites [40]. It has also been used for the production of heavily nitrogen doped carbon onions, centred on the azofullerene $C_{48}N_{12}$ [41].

Based on theoretical studies ion implantation has been proposed as a way to selectively dope carbon nanotubes with nitrogen [42, 43]. Recently this approach was used experimentally to implant nitrogen in MWNTs [44]. The tubes were deposited on silicon substrates and bombarded with low-energy N_2^+ (0.5 keV and 15 nA/cm^2). They quantified the nitrogen concentration to be 0.47 at% using XPS. Yamamoto *et al*.[45] tried to dope SWNTs using mass separated nitrogen ions, unfortunately however it seems that the tubes are destroyed before the actual incorporation of nitrogen.

We anticipate that more work will be carried out using ion bombardment to dope tubes, since it has several advantages over doping during growth. In particular spatially resolved doping should allow both homogenous dopant distribution and

spatially localised doping as required. Notably, concentration variances in nanotubes doped during synthesis can arise from inhomogeneous synthesis conditions, e.g. impurities in the catalyst, catalyst size, an uneven gas flow, or temperature gradients in the reaction zone.

1.3.4 Growth parameters governing doped nanotubes

It is nearly impossible to draw parallels between doping of multi-walled tubes synthesised via high temperature routes and CVD methods. This has to do with the fact that these methods are fundamentally different since with CVD methods it is essential to use a catalyst which is not the case for high temperature methods. In this section we will restrict ourselves to comment on the growth mechanism for CVD synthesised tubes.

A major challenge is to understand the growth mechanism on a microscopic scale. Parameters generally accepted to be important for the synthesis of undoped carbon nanotubes are:

- Catalyst material
- Catalyst particle size
- Catalyst support
- Precursors
- Gas feedstock
- Pressure and flow of gas feedstock

For the synthesis of doped nanotubes further parameters are added to the list. It is necessary to consider the difference in interaction energy between the dopant species and the carbon species with the catalyst and support material. To further complicate the discussion, as can be seen from Table 1 most groups when synthesising doped

nanotubes use complex molecules as their carbon and nitrogen feedstock, and even mixtures of molecules. This significantly complicates the issue, particularly since to date no studies that we are aware of have been aimed at elucidating the mechanism whereby feedstock molecules are broken down.

In a study of catalyst behaviour, nitrogen-doped tubes were synthesised by the pyrolysis of acetonitril over solid solutions of Ni/Co with different stoichiometries ranging from pure cobalt to pure nickel. A strong correlation between catalyst composition and nitrogen concentration in the tubes was observed. The highest nitrogen concentration in the nanotubes was observed in the sample with a catalyst stoichiometry of 1:1 and it was suggested that this was because the nitrogen solubility is also the highest in this catalyst. A similar nitrogen concentration was observed in the tubes synthesised with pure nickel as the catalyst, and the authors correlated this with the observation that nickel provides the highest MWNT growth rate [33].

Many studies demonstrate that nitrogen often is found in higher concentrations in the interior walls of the nanotubes [3] . The group of Park showed by XP spectroscopy that by using increasing photon energies the signal for nitrogen increased thus the inner walls of the tubes have a higher nitrogen concentration; they demonstrated this phenomenon for both double-walled tubes [3, 46] and multi-walled tubes [47]. The same group correlated the concentration of nitrogen in the inner walls to be a direct consequence of stability, based on calculations. We think that the higher nitrogen concentration in the inner walls is more likely to be a consequence of the different interactions between the nitrogen specie and the carbon specie within the catalyst.

From EELS peak intensities, Sen *et al.* [48] found nitrogen concentrations of C:N ratios of 3% and 9% in two different tubes from the same sample. Other groups have also observed high variance in the nitrogen concentration in different tubes in the same sample, varying between ~6 at% and ~16 at% [2]. Such concentration variances must arise from inhomogeneous synthesis conditions, e.g. impurities in the catalyst, catalyst size, an uneven gas flow, or temperature gradients in the reaction zone.

In order to clarify the role of the various parameters further studies are needed with emphasis on the morphology of the tubes, which depends on the actual growth mechanism. The discussion above makes it clear that the growth mechanism must depend critically on the catalyst chemistry, which depends on many factors.

1.3.5 Nitrogen-doped carbon nanotube morphologies

As-grown doped SWNTs exhibit morphologies similar to their undoped counterparts, namely straight unbuckled nanotube walls [1, 13] . Defects are observed but not necessarily correlated to the nitrogen dopants, however substitution reactions of pre-grown pristine SWNTs leads to more deformation in the nanotube walls than as-grown nitrogen doped SWNTs [39]. A typical example of nitrogen-doped SWNTs is shown in Figure 2e.

Unlike SWNTs, nitrogen-doped MWNTs exhibit very distinct morphologies significantly different from their undoped counterparts. In nearly all cases these tubes have a so-called ‘bamboo’ structure, where the nanotube contains a regularly spaced array of internal carbon walls; alternatively ‘nano-bell’ structures where the tube appears to be a stack of linked droplet shaped cavities. The alignment and number of nanotube walls depends on dopant concentration and catalyst used, and the walls are

often more buckled and irregular than those of undoped MWNTs. The connection between different 'nanobells' segments are often weak, with graphitic layers terminating on the surface of the next section [49]. Representative examples of the morphology of N-doped SWNTs and MWNTs are given in Figure 2.

One example exists in the literature demonstrating that low concentration nitrogen doped MWNTs (~3%) can have extremely well ordered morphologies but still differ significantly from their undoped counterparts [50, 51]. These tubes are extremely straight with a very high degree of internal order: the tubular layers are of the same helicity and the tube interwall distances (c/2 spacing) appear to correspond to graphite by being in crystallographic register and not having the turbostratic carbon distance usually observed in MWNTs. These exciting results have yet to be reproduced by other groups.

Conventional nanotube growth models cannot explain the regular internal 'bamboo' cavities of nitrogen doped MWNTs. An alternative growth model is proposed for these nitrogen-doped tubes. The metal catalyst is forcefully ejected from the tube interior due to stress accumulated in the graphitic shells (see for example [52-54]). In this case doped graphitic shells form on the surface of the catalyst particle parallel to the catalyst surface. As the number of layers increases this pressurises the catalyst particle until it is ejected from the cavity and the process begins once again. This model is supported by the observation that a decrease in the catalyst particle size decreases the bamboo periodicity [55]. This model may not be universally applicable however since it requires a uniformly decreasing interior carbon wall diameter, which is not always the case [30].

In an interesting experimental study nickel and iron catalysts were compared, with resultant multi-walled tube morphologies showing either straight (Ni) or buckled (Fe) walls. This was explained in terms of nitrogen solubility in the catalyst; nitrogen is very soluble in iron whereas in the case of nickel it would be forced to diffuse over the catalyst surface [55]. It is likely that the different nitrogen-doped nanotube morphologies as compared to undoped tubes are due to nitrogen solubility in the catalysis, diffusivity in the catalyst bulk and on its surface, and competition for carbon interstitial and surface sites at the catalyst. Interestingly, a second study of Ni/Ni:Fe catalysts showed a bimodal distribution of N-MWNT diameters when using pure nickel catalysts, indicative of two types of carbon nanotubes with average diameters of 18 and 60 nm respectively. With a mixed Ni/Fe catalyst a uniform diameter distribution around 50 nm was found [56].

Another common feature of nitrogen-doped multi-walled nanotube samples is the presence of tightly coiled 'telephone cord' nanotubes (see for example Figure 3). Yudasaka *et al.* observe that the tips of N-doped nanotubes often form coils, with thinner tube regions and coiled tips often displaying nodes [30]. These coils are often taken as an indication that nitrogen facilitates regular inclusion of pentagons into the graphite network, a conclusion supported by various theoretical calculations (see below). However such tubes are sometimes also seen in ostensibly undoped samples [57, 58] and have been linked to choice of catalyst [59].

Note that although unusual tube morphologies such as winded tubes and tubes with thin foils or lamellae growing perpendicular to the tube axis have been observed in

very large diameter N-doped MWNTs [60], these are probably due to folded or rolled up graphene sheets, rather than conventional nanotubular structures.

1.3.6 Nanotube Helicity

Helicity selective growth of nanotubes would be a major breakthrough for nanotubes future application, since helicity is the determining factor in the electronic and optical properties of single-walled nanotubes. Graphite is a semi-metal since the valence and conduction bands states touch at the K points in the Brillouin zone. Rolling graphite into a nanotube reduces its dimensionality since the system is now only periodic along the tube length, and hence the 2D Brillouin zone of graphite is collapsed into a 1D line. If this cuts through the original graphite K point then the tube will be metallic and otherwise it will be semiconducting. The orientation of this line, and hence whether a nanotube is metallic, semi-metallic or semiconducting, is determined by the tube helicity [61].

The first paper their dealt with the possibility of using dopants as a helicity growth enhancer was published by Blase *et al.* in 1999 [62]. It was experimentally and theoretically shown that boron in MWNTs gives rise to a preferred zigzag or near zigzag helicity. It would be tempting to propose a similar helicity selection during growth of nitrogen doped tubes. However HRTEM electron diffraction studies of CN_x MWNTs produced by pyrolysis shows no preferential helicity [63]. Recently it was experimentally demonstrated by Koziol *et al*. that in low nitrogen doped MWNTs a crystallographic register exists between the different nanotube layers [64]. Figure 3 shows the electron diffraction patterns of undoped and nitrogen doped multi-walled nanotubes in their samples, clearly indicating the crystallographic register.

A recent study combining Raman and absorption spectroscopy demonstrated a helicity dependent change in the relative abundance of SWNTs due to the combined presence of nitrogen and boron, with nitrogen alone having none or nearly no influence on the preferred geometrical helicities [65]. A correlated investigation by Li *et al*. combining Raman and photoluminescence-excitation spectroscopy showed that the nitrogen and nitrogen/boron doping of SWNTs significantly changed both their optical properties and diameter distribution [66]. Smaller diameter tubes are preferentially formed in presence of boron and nitrogen significantly change the emission properties of the nanotube ensemple. The latter is most likely due to different bundling structure in solution compared to undoped nanotubes. Only very small changes are observed in the emission energies for individual nanotubes.

The theoretical knock-on effect on nitrogen doping was shown by Nevidomskyy *et al.* whose density functional (DFT) calculations of substitutional nitrogen (0.26% to 1%) in nanotubes of different helicity showed significant changes in behaviour [67]. In a semiconducting (8,0) nanotube, the state associated with the nitrogen was localised to within 30 Å for 90% of the spin density, leading to a chemically and electronically active defect. However in a metallic (5,5) nanotube, the state was delocalised. They noted that as substitutional nitrogen approach one another in metallic nanotubes, their interaction will oscillate depending on whether their spin density maxima coincide or not. This will not be the case in semiconducting tubes where the spin density occurs on different sublattices on the two sides of the nitrogen atom, and so maxima will never coincide, see Figure 4.

As seen from above, experimental evidences of helicity selected growth for doped tubes is always elucidated from electron diffraction. A single theoretical paper deals

with the possibility of utilising XPS to get knowledge of the helicity for nitrogen doped tubes. Their computational modelling of substitutional-nitrogen doping suggests a helicity dependence of the N(1s) binding energy and associated XPS signal [68] , with calculated N(1s) binding peaks at 401.9 eV for substitutional nitrogen in a (7,7) armchair nanotube and 403.3 eV in (12,0) zigzag and (10,4) chiral nanotubes.

1.3.7 Nitrogen molecules in tubes

Several authors have recently started to discuss the possibility of intercalated nitrogen molecules in between the layers in nanotube, this discussion was commenced for two reasons: *i*) Several groups have observed a signal corresponding to nitrogen gas by EELS and XPS [29] [49]. This can possible be explained by an inclusion of nitrogen in the tube interior during synthesis or that during the XPS or EELS characterisation a gradual degradation of the walls occur and a reaction of two nitrogen species takes place and form nitrogen gas. Choi *et al*. calculates that the intercalation energies for nitrogen gas and compare it to the dissociation energy of C-C bonds in CNTs and thereby conclude that it is possible to intercalate N_2 in between the walls, unfortunately the authors did not report on the interlayer spacing [47]. *ii*) A couple of group have observed a significantly changed distance between the graphitic layers of nitrogen doped tubes. Koziol *et al.* saw that the distance, in extremely well graphitisized MWNTs with a low nitrogen concentration, corresponds more to the graphitic distance (3.35 Å) than the turbostratic distance (3.4 Å) typical for undoped MWNTs [64]. The same group also studied more disordered nitrogen-doped MWNTs and reported an increased interlayer spacing on around 12-14% [51] compared to the interlayer spacing normally observed in undoped nanotubes.

There is helicity dependence in the transport characteristics of nitrogen doped nanotubes due to their intrinsic metallic or semiconductor character (see Transport section below). However Lammart *et al.* [69] found in their doping calculations that for realistic doping concentrations and distributions, semiconducting and metallic tubes behave similarly. This is because the metallic tubes have low near-constant density of states across the Fermi level which forms a relatively inert background compared to the strong density variations due to doping.

1.4 High concentration nitrogen doping and the quest for C_3N_4

Although the bulk of the review concentrates on isolated or clustered nitrogen defects it is possible to imagine nanotubes grown from tubular arrangements of metastable CN_x-phases, and the studies of CN_x-phases in thin films provide valuable insight into possible structural arrangements of nitrogen doped CNTs.

The quest for C_3N_4 began after it was postulated that α-C_3N_4 or β-C_3N_4, by structural analogy with Si_3N_4, could be "ultra-hard" phases and may even be harder than diamond. The extreme properties of C_3N_4 were supported by calculations of Cohen in 1985, who calculated a semi-empirical bulk modulus between 461 and 483GPa, significantly larger than that of diamond [70].

Bulk modulus is not necessarily a good indicator of comparative hardness, and indeed Teter observed that a better predictor is the shear modulus [71]. Most of the 3D crystalline proposed phases of C_3N_4 also have high shear moduli, but not in excess of diamond [72].

After these initial C_3N_4 structures were proposed, a wide range of alternatives have appeared in the literature, often using graphitic, Si_3N_4 or other more complex mineralogical phases as analogues. These include a spinel phase [73] [74], a "pseudo-cubic" phase [75, 76], and a cubic C_3N_4 phase [74]. These are described in more detail in an excellent review by Kroke and Schwarz [71]; none have been unambiguously synthesized and characterized to date.

Amongst these predicted phases are a number of graphitic layered structures, primarily postulated as useful intermediate structures which could be transformed into ultra-hard crystalline phases via high pressure treatments. Once we allow for other stoichiometries, a wide range of layered C_xN_y structures are possible, all of which are potential candidates for new phase high nitrogen content nanotubes. These can be classified into several broad families which are detailed below (Figure 5).

We emphasise that none of these phases have been synthesized and characterized as nanotubes to date. They instead provide insight into possible structures present in highly doped tubes, and serve as potentials goals in the quest for single phase C_xN_y nanotube structures.

1.4.1 Monolayer CN_x phases

Ortega and Sankey first considered a graphitic C_3N_4 phase consisting of s-triazin units (hexagons of alternating pyrridinic-N and C) linked via planar trivalent nitrogen [77]. Teter and Hemley also proposed a hcp graphitic C_3N_4 phase [74] , and there are a number of possible sheet stacking orientations of these layered materials [75]. The relative stability of these structures at varying pressure was investigated by Lowther, showing low energy phase transitions are possible [78]. A lower energy graphitic

C_3N_4 phase (by ~30kJ/mol) was later proposed [79], utilising s-heptazine units instead of s-triazine.

It is possible to imagine a parallel family of structures created using orthorhombic rather than hexagonal unit cells, altering the distribution of 2- and 3-fold coordinated nitrogen [80]. Mattesini *et al.* [81] surprisingly show this orthorhombic phase to be more metallic than the hexagonal phase, with little difference in energy between the two arrangements. This is despite the lack of aromaticity in this structure, which would be expected to destabilise the structure and encourage non-planarity of the nitrogen [71].

All of the structures discussed thus far can be considered CN_xV_y variants, *i.e.* monolayers of hexagonal CN with varying concentrations and arrangements of vacancies. More complex structures with larger pore sizes have also been proposed [71, 82] using carbodiimide (>N-C≡N) or cyanamide (-N=C=N-) [71] bridging group between s-triazin and s-heptazine units, however such low density phases are unlikely to have the structural rigidity or chemical stability to form tubes.

A general schematic of all the phases discussed thus far is given in Figure 6. By allowing deviation from C_3N_4 stoichiometry, a wider family of monolayer phases are possible.

Monolayer phases with stoichiometries other than C_3N_4 have also been proposed, notably CN (Figure 6a,b) [83] and $C_{11}N_4$ (Figure 6e,f) [84]. CN (alternate graphite site substitution by nitrogen) is non-aromatic leading to buckling, and should be

highly chemically reactive. Semi-empirical calculations of CN tubes found the most stable arrangement to be a zigzag oriented tube with C-N bonds parallel to the tube axis [85], with modulation along the tube length corresponding to two populations of nitrogen atoms, only half of which contribute to the π system. Density functional modelling of CN nanotubes found them to be metallic but thermodynamically unstable compared to C_3N_4 tubes, which were insulating [86]. $C_{11}N_4$ was proposed based on experimentally observed nitrogen concentrations, and has some unusual properties, notably being isoelectronic with diamond; although only orthorhombic phases are considered in the literature it is also possible to imagine hexagonal variants.

Once non-C_3N_4 stoichiometries are considered, and in addition allowing for double and triple bonded species such as carbodiimide and cyanamide groups, there is a large family of monolayer CN_x structures possible. A systematic, and possibly automated theoretical study to draw definitive energetic conclusions concerning these would be useful.

1.4.2 Bilayer CN_x phases

In addition to 'graphitic' monolayer structures, it is possible to imagine other layered structures with out-of-plane bonding and finite thickness. Out-of-plane bonding allows for sp^3-coordinated atoms, opening up many new potential layered phases.

Bilayer phases have not been explicitly discussed in the context of nitrogen-doped nanotubes but are good potential candidates, for example for the nitrogen rich inner layers of doped multi-walled nanotubes.

Côté and Cohen [87] studied various CN structures with 1:1 stoichiometry including structures based on the atomic arrangement in GeP [88], β-InS and GaSe. The most stable was found to be the GaSe structure, a semiconducting phase consisting of bilayers of alternate C and N with carbon cross-links between them (shown in Figure 7). This should be significantly more stable than the monolayer CN phase discussed above. Various gallium selenide stackings are possible, and combinations of mono and bi-layer CN structures could be imagined, such as based on the structure of GaTe [89]. These phases will be non-aromatic with wide band gaps due to the complete sp^3 bonding.

Amongst other structures, a layered C_3N phase consisting of C-C cross-linked bilayers was proposed by Sandré *et al.* [90] (Figure 7c), containing a mixture of sp^2 and sp^3 carbons.

1.4.3 Hydrogen incorporation

Hydrogen is extremely difficult to detect and is rarely if ever considered when discussing potential CN_x phases in heavily nitrogen doped nanotubes. Nonetheless it is often present during growth, either as a gas phase impurity or within the feedstock gas species such as methane, ethylene, ammonia, and acetonitrile. Within the C_3N_4 literature there are many stable $C_xN_yH_z$ polymers, notably 'melon', $[C_6N_9H_3]_n$ (see Figure 6g). It has been suggested that many supposed bulk C_3N_4 phases may in fact be mischaracterised melon, or other molecular or polymeric crystalline $C_xN_yH_z$ phases [72].

The role of hydrogen in nitrogen doped nanotube growth has not been discussed in the literature to date. Nonetheless, adding hydrogen to the equation clearly opens up a wide range of new potential layered structures.

1.4.4 Mechanical properties of new phase C_xN_y nanotubes

Within the C_3N_4 literature it is often noted that the proposed ultra-hard C_3N_4 phases, although predicted to possess exceptional mechanical properties, are unlikely to be as hard as diamond [71]. In addition this refers to the crystalline phases such as cubic- and zincblende C_3N_4; the graphitic phases are much softer and considered instead as suitable precursors for the synthesis of hard C_3N_4 phases [72]. Thus there seems little motivation for trying to grow graphitic C_3N_4 nanotubes for their mechanical properties (although we note that some of the bilayer and crystalline tubular alternatives discussed above may have improved mechanical properties). Tight binding calculations show a Young's Modulus for C_3N_4 SWNTs of around half that of pure carbon tubes, due to the highly porous lattice structure [91, 92], a reduction also reflected in empirical pair potential calculations [93]. However there may be other useful properties of such materials that could be engineered in. Guo and Goddard speculated that α-C_3N_4 would be auxetic (have a negative Poisson's ratio) [94], and it is possible to imagine graphitic C_xN_y structures that would also be auxetic, raising the curious possibility of nanotubes whose diameters increase under tension.

1.5 Structure and electronic properties of nitrogen in carbon nanotubes

Nitrogen doped MWNTs have a strong nitrogen state just above the Fermi level [17, 18]. In addition they exhibit unusual growth morphologies as compared to their undoped counterparts. It is clear that nitrogen is having a profound effect on the structural arrangement and electronic properties of the nanotubes. There have been many theoretical studies of the bonding configuration of nitrogen within carbon nanotubes in order to explain these unique properties of nitrogen doped tubes.

Various structural models have been proposed for the bonding configuration of nitrogen doping in carbon nanotubes. There are three primary candidates: pyridine-like, where the nitrogen atom is two-fold coordinated (Figure 8a), pyrrole-like where although substitutional it sits in a five-fold ring (Figure 8b), and 'graphitic' or substitutional where it replaces a graphitic carbon atom (Figure 8c).

More specifically, pyridinic in this case is used to refer to nitrogen atoms contributing one p electron to the π-system, pyrrolic referring to nitrogen atoms with two p-electrons in the π-system (not necessarily in a five-membered ring as in pyrrole). It should be noted that pyrrolic nitrogen is sp^3 coordinated. Graphitic nitrogen sits in-plane, replacing a graphitic host carbon atom. Since it is under coordinated in this arrangement it is expected to act as an electron donor. Pyridinic and graphitic nitrogen are both sp^2 coordinated.

Compound structures have also been considered, notably nitrogen-vacancy complexes containing pyridinic two-fold coordinated nitrogen atoms neighbouring a carbon vacancy (hereafter referred to using the letter V). These include NV [33, 42, 95] , N_2V [33] and N_3V (see Refs [18] and [33], and references therein, Figure 8f/g). Other nitrogen defects considered include 'interstitial' divalent nitrogen atoms (which form a bridge over a broken graphitic C-C bond, Figure 8h) [96, 97], neighboring substitutional nitrogen pairs [95, 98], and nitrile -C≡N (sp hybridised nitrogen, Figure 8d) which has been proposed in various CN_x thin film structures.

Robertson and Davis provide a chemical bonding argument why pyridine-like and pyrrole-like nitrogen are non-doping in sp^2 networks whereas substitutional nitrogen generates a donor state. Their bonding diagram is reproduced below (Figure 9). A carbon atom in graphite has four bonded valence electrons, three forming sigma bonds and one forming an aromatic π-bond with its neighbours (Figure 9a). Considering instead a nitrogen atom with its five valence electrons; in a pyridine-like arrangement two of these electrons form sigma bonds, two forms an in-plane filled p_x-like non-bonding state, and the fifth forms a π-bond with its neighbours, thus giving a filled valence band (Figure 9b). For pyrrole-like bonding, three of the nitrogen valence electrons form sigma bonds and the remaining two are donated to the pi-bond around the 5-fold ring, which now has 6 electrons and is aromatic (Figure 9c). Substitutional N uses three electrons in sigma bonds, one to pi-bond and is unable to use its fifth electron for bonding, forcing occupancy of a π*-donor state (Figure 9d). It is therefore the only one of these configurations to contribute electrons to the sp^2 network. Note however that this does not preclude pyridinic defect complexes from having corresponding acceptor states. For example, pyridinic nitrogen next to a

carbon vacancy (N_xV, x=1,3) will have an acceptor state due to the missing p_z orbital of the vacancy and corresponding creation of a π-radical. This chemical bonding model is quite simplistic and should serve only as a useful indication to nitrogen behaviour, since in practise there will be strong interactions with graphitic host states of the same symmetry.

Direct substitution of carbon in a nanotube wall by nitrogen was first theoretical studied by Yi and Bernholc using density functional theory (DFT) [99]. They studied semiconducting zigzag (10,0) and chiral (6,5) nanotubes, finding an impurity state 0.27 eV below the conduction band at Gamma. The donor state overlapped between cells since nitrogen atoms were only at 8.4 Å spacing (1.3%). Lammert *et al.*treated theoretical disordered substitution in (8,0) nanotubes at a nitrogen concentration of 1.4%, and found donor states localised within around 10 Å [69]. More recent DFT calculations by Nevidomskyy *et al.* [100] in much larger supercells confirm the presence of a donor state associated with substitutional nitrogen at around 0.2 eV below the conduction band in zig-zag (8,0) nanotubes, and around the same energy in armchair (5,5) nanotubes.

There appears to be little structural relaxation associated with nitrogen substitution, for example Yi and Bernholc [101] report based on their calculations shifts of less than 0.02 Å during geometrical optimisation after substitution (N-C bond lengths of ~1.43 Å), confirmed by the current authors [102], although Zhao *et al.* find 0.04 Å bond shortening for substitutional nitrogen in a (5,5) nanotube compared to carbon [95].

In contrast to substitutional nitrogen, tight binding calculations of pyridinic N show it has a non-doping state below the Fermi level [103]. There have been several studies of pyridinic nitrogen replacing one of the three carbon atoms neighbouring a vacancy, referred to hereafter as a nitrogen-vacancy (NV) complex. DFT studies of a NV complex in (5,5) nanotubes show reconstruction of a weak carbon-carbon bond between the two carbon neighbours of the vacancy [43], similar to that reported for the carbon vacancy in graphite [104], but with stronger reconstruction (1.88 Å) due to tube curvature. The curvature also imposes a preferential orientation on the NV defect with the reconstructed C-C bond as close to circumferential as possible in order to minimise its length. Modified DFT calculations give C-N bond lengths of 1.34 Å, with an associated acceptor state just below the Fermi level [95].

Calculations by Kang and Jeong [98] of the N_3V structure show impurity states 0.5 eV below Fermi energy (E_F) similar to NV. It seems likely the donor states originally reported for the N_3V structure [17, 18] were due to inaccurate tight binding parameterisation.

Other groups have theoretical examined interstitial nitrogen, which sits divalent on the nanotube surface, bridging an underlying broken C-C bond [42] . This was shown to have a strong acceptor state [94, 96]. However its surface migration barrier calculated using DFT is only 1.1eV [43] and it will thus be mobile at room temperature, with only a short lifetime before combining with other defects or forming N_2.

It has also been suggested that nitrogen may decorate open tube ends with pyridine-like rings [105]. Another possibility for pyridinic nitrogen incorporation in MWNTs

without the addition of carbon vacancies is nitrogen decoration of dangling sheet edges within the tube walls. Nanotube wall corrugation and sheet mismatch is a common feature of high resolution transmission electron microscopy (HRTEM) images of nitrogen doped MWNT walls [106]. This has not been explored either theoretically or experimentally as far as the authors are aware.

Molecular dynamics simulations (modified Tersoff potential) of nitrogen ion irradiation [42, 43] suggest that up to 40% of impinging nitrogen can easily enter the lattice in substitutional positions, with a small minority of NV defects. Tight binding calculations of nitrogen impacting on vacancies found direct substitution only for curvature equivalent to tube diameters larger than 8 nm [19]. For higher curvatures the vacancy semi-'heals' with two new pentagons and a 4-fold carbon [107], blocking nitrogen access to the vacancy site. Although important for low energy nitrogen bombardment, the model does not consider higher energy ion impact or nitrogen incorporation directly during wall growth.

1.6 Spectroscopy of nitrogen in carbon nanotubes

1.6.1 Electron Energy Loss- and X-ray Photon Spectroscopy

Comparison of spectroscopy carried out on nitrogen-doped carbon nanotubes with that of nitrogen doped carbon thin films shows many similarities, and it is likely that nitrogen behaves similarly in the majority of carbon systems. However nanotubes provide a more controlled structural architecture than that of amorphous or semi-amorphous thin films, and it is hoped that improved understanding of nitrogen bonding in nanotubes will also help resolve some of the ambiguities in structural

assignment within nitrogen rich carbon thin films. The exception to this is the likelihood of nitrile surface groups in many CN_x thin films, which do not seem to be observed in N-CNTs (discussed further below).

Experimental core EELS studies of nitrogen doped SWNTs and MWNTs show similar peak splittings for the nitrogen and carbon *K* edges as observed in CN_x thin films. In SWNTs the nitrogen *K*-edge is seen to split into two distinct π^* peaks at 398.6 and 402 eV [1, 22], see Figure 10.

For heavily N-doped MWNT samples these two peaks are observed along with two additional peaks, [108]. Analysis of the nitrogen distribution within the tubes shows these additional peaks occur within the interior walls of the MWNTs associated with a less sp^2-C 1s signal, and are possibly due to either inter layer cross-linking or a new N-rich CN_x phase. Other EELS studies of nitrogen doped MWNTs only reveal the same two peaks (398.7 and 400.7 eV) as for SWNTs [18]. Spatially resolved EELS analysis of MWNTs shows a variety of different behaviours [96]. The carbon *K*-edge varies through a cross-sectional slice of CN_x nanotubes, showing more graphitic character in the outer layers. The N *K*-edge depends on the catalyst used, and notably in this case only one N 1s peak was observed for each catalyst type. For Ni catalysts a broad peak at 401-404 eV is seen whereas for Fe catalyst a sharper 398 eV peak is seen, the EEL spectra are given in Figure 11. In regions of higher nitrogen the carbon π^* peak intensity decreases. It is not clear whether this is due to decreased sp^2 character in the carbon or a filling of the π^* state by excess nitrogen electrons [85].

Droppa *et al.* [109] combined XPS, EELS and Raman of bamboo-like N-CNTs, observing three XPS peaks at 397.9eV, 398.6 eV and 400.5 eV, with the 398.6 eV peak intensity dropping with increasing nitrogen concentration. Their EELS signal also showed a π^* peak in the nitrogen signal from bamboo regions, at around 408 eV.

Large diameter CN_x nanotubulites also showed two N(1s) peaks in EELS at 399 and 401 eV, with the 399 eV peak intensity increasing with increasing oxygen content [40] . The 0.7eV resolution restricted ability to resolve any finer peak splittings, if present.

There have been many XPS studies performed of N-doped CNTs. N 1s spectra for N doped MWNTs grown from Ni, Ni/Co or Co catalysts are shown in Figure 12 [68]. These spectra were successfully fitted with three Gaussian functions at ~399.1, 401.4 and 402.7 eV.

Yudasaka *et al.* [30] first showed N doping of CNTs through XPS with two N1s peaks at 399.0 and 401.0 eV from CVD at 900°C. At 800°C these peaks shifted to 398.6 and 400.7 eV. Other groups have also reproduced this N1s peak splitting at 398.7 and 400.9 eV [18][110]. Sen *et al.* find a N1s XPS signal at 401eV for MWNTs grown from pyridine pyrolysis, although spectral resolution precludes identification of any secondary peaks [48]. Although XPS can provide a great detail of information on local bonding environments, one should take great care using bulk measurement techniques which reflects average properties of the sample for probing the hetero atoms in the nanotube samples which basically always contains impurities.

Peak assignment is as controversial and as varied as for CN_x thin films, and indeed many of the assignments have been taken directly from this field. Wang *et al* use XPS to identify three peaks at 398.1 eV (weak), 401.0 eV (strong) and 405.1 eV (strong) in well ordered compartmentalized bamboo MWNTs with [N] ~9% [111]. These are assigned to pyridinic, pyrrolic and graphitic nitrogen, based on the theoretical assignments of Ref. [112]. Assignment of the peak at 401eV to pyrrolic-type nitrogen is supported by studies of the azo-fullerene $C_{59}N$ which exhibits a N 1s XPS peak at 400.7 eV [27] . For other possible peak assignments we refer the reader to the section on spectroscopy of CN_x thin films above.

Jiménez *et al.* [113] examined N1s X-ray absorption near edge spectroscopy (XANES) peak heights with varying temperature in CN_x thin films. Four peaks were identified at 397.8, 399.1, 400.7 and 403.5 eV. The 397.8 eV peak increased in intensity from 200 to 400°C, apparently at the expense of the 403.5 eV peak and to some extent the 399.1 eV peak. This could be consistent with, for example, vacancy trapping by nitrogen. While the 403.5 eV peak has disappeared by 400°C, over all temperatures up to 1150°C there is a gradual increase of the 400.7 eV peak. A similar temperature study of nitrogen doped nanotubes would be useful, particularly if combined with vacancy rich nanotubes (e.g. through irradiation).

1.6.2 Vibrational spectroscopy – Infrared and Raman spectroscopy

Raman spectroscopy is a very powerful technique for undoped nanotubes since using this method it is possible to get information about the physical and electronic structure of the samples. Therefore it could be envisioned that the technique will be equally efficient for characterising substitutional doped tubes. Using Raman spectroscopy Lim *et al*. [114] noticed a significant down shift of the graphite peak from 1589 to

1580 cm^{-1} upon nitrogen doping. At the same time they observed a significant increase of the ratio of the intensities of the defect and graphitic peaks (I_D/I_G). Usually the ratio I_D/I_G is interpreted as a measure of the degree of order of the material. The intensity change of the I_D/I_G ratio was confirmed in a thorough experiment by Maldonado *et al.* [115]. The correlated XPS results with Raman scattering measurements for a row of samples with increasing nitrogen concentrations (0 atom% to 10 at%) and noticed that the ratio of the D (defect) and G (graphite) bands integrated intensities scaled nearly linearly with the nitrogen concentration inferred from XPS, see Figure 13. The change of I_D/I_G ratio of nitrogen doped MWNTs compared to their undoped counterpart have been observed by several other groups [109, 116-118].

Q.-H. Yang *et al*. [119] observed significant shifts of both the D and G band for both boron and nitrogen doped multi-walled nanotubes. For nitrogen doped nanotubes they observed a down shift of the G bands as already discussed but they also noticed an up-shift of the D band. The down shift of the G band was explained by a decrease of the electrical resistivity regardless of the nature of the dopants.

So far only a couple of infrared spectroscopy investigations of nitrogen doped multi-walled tubes have been reported. Misra *et al.* [120] investigated nitrogen doped tubes synthesised by microwave plasma CVD and observed a wide range of vibration bands which were interpreted as belonging to chemically bonded impurity and nitrogen species. The most significant observations were the bonds at 1250 cm^{-1} and 1372 cm^{-1} which were assigned to -C-N and -N-CH_3 respectively and both bands were gradually suppressed *via* thermal treatment. A similar study was carried out by *Wu et al.* [121] they correlated the peaks at 1119, 1266 and 1400 cm^{-1} to C-N stretch vibration; the

peak at 1596 cm^{-1} to C=N; and 2079, 2177, and 2351 cm^{-1} to nitrile groups. Additionally a broad vibrational band at 3420 cm^{-1} was detected which was tentatively assign to NH and/or NH_2. Chan *et al.* [122] measured the infrared spectra of nitrogen doped tubes synthesized by a post treatment route where carbon nanotubes were exposed to high input power nitrogen plasma using a microwave plasma enhanced chemical vapor deposition system. They observed a chance of the signal frequency and intensity as a function of exposure time to the nitrogen plasma. The band assigned to N-C stretching moved from 1130 to 1235 cm^{-1} and the band assigned to the C=N stretching mode changed from 1590 to 1610 cm^{-1} with increased doping concentration. In the same work the authors did not register the characteristic C≡N stretching vibration at around ~2200 cm^{-1}.

1.6.3 Spectroscopic modelling of nitrogen in carbon nanotubes

Spectroscopic peak assignment is often performed by comparison with well characterized small molecules. Many spectra are available in the literature, including N(1s) binding energies for various molecules [123] [103], and polymeric solids [124] with nitrogen in different bonding configurations . However the use of small molecules as reference states for solids is discouraged, since they do not satisfactorily account for initial-state charge transfer or final-state screening in core level shifts, particularly for π-conjugated systems [124]. The alternative is to turn to solid state theoretical calculations.

There are different techniques for calculating XPS N(1s) binding energies, including the delta self-consistent-field (Δ-SCF) technique [125][112, 126] and those based on

Koopman's theorem [33]. EELS core-loss spectra are typically calculated from the local *p*-projected density of states.

To date there have been various calculations to aid in assignment of these spectral nitrogen peaks. The calculations which have been taken as reference for some time were performed by Casanovas *et al.* [112] in 1996. Hartree-Fock studies of AM1 optimised nitrogen structures in different graphitic molecules led to the assignment of three different nitrogen species, pyridinic at ~399.0 eV, pyrrolic at ~400.3 and graphitic at ~401-403 eV (three sp^2-carbon neighbours) respectively. These values are calculated from ground state wavefunctions and shifted by 3.2 eV to allow for the difference in relaxation energies of the C 1s and N 1s core-holes. Notably the highest peak showed a large spread of values depending on cluster size and atom position.

Hellgren *et al.* [127] use soft X-ray absorption spectroscopy (SXAS) and emission spectroscopy (SXES) to identify these peaks in carbon nitride thin films. Accurate modeling (using gradient corrected DFT with full core-hole and frozen core state orbitals) was used to calculate spectra for different nitrogen environments and compared directly with their experimental spectra. On the basis of this modeling they assign peaks at around 398.5 eV to pyridine-like N, ~401 eV ascribed to nitrogen substituted (either graphitic or pyrrolic), and 399.5 eV to C≡N (nitrile). They note that difference in the coordination of nearest or second nearest C neighbours only cause slight changes in the peak positions and spectrum shape (i.e. pyrrolic and graphitic show approximately the same spectral features). However C≡N seems an unlikely candidate in nanotubes since combined XPS and FTIR studies show no FTIR absorption at ~2200 cm^{-1} characteristic of C≡N stretching [122].

Bulusheva *et al.* [68] fitted their N-doped MWNTs XPS signal with three peaks at 399 and 401.4 eV and a weaker peak at 402.7 eV. Theoretical Hartree-Fock modelling of (7,7), (12,0) and (10,4) tubes containing substitutional N and N_3V pyridine-like species showed a strong helicity dependence of calculated XPS signal for the substitutional nitrogen (N_s), suggesting their three peaks were due to N_3V, N_s in armchair tubes, and N_s in zigzag or chiral tubes respectively.

The same group also performed accurate 6-31G* Hartree Fock calculations on the complexes N_xV (x=1,2,3) and N_s in small graphene sheets, calculating chemical shifts using Koopman's theorem and correcting for photoionisation electron relaxation by using a correction factor based on known small molecule excitations [33]. They obtained calculated peaks at 401.68eV (N_s), 399.04 a(N_3V), 400.12 (N_2V) and 400.62 (NV).

Calculations on molecular systems containing pyridine-like N showed a downward shift of the N(1s) ionisation potential as the aromatic molecular fragment size increases [123]. This emphasises the importance on the measured N(1s) peak of not just the nitrogen bonding, but also the nature of its surrounding environment. Their molecular calculations predict a chemical shift of the C (1s) peak of around 1 eV for each additional N neighbour, but bulk phase calculations show weaker shifts. Their bulk calculations give pyridinic nitrogen at 398.3-398.9 eV, pyrrolic N at 399.8 eV and substitutional N between 400.8-402.4 eV with higher values for more graphitic environments. Similar cluster size dependence of binding energy was observed in Hartree-Fock optimised clusters using Δ-SCF for the chemical shifts [126].

Unfortunately with the variety of models available producing very similar predicted binding energies it is difficult to make an unambiguous theoretical assignment of the observed N(1s) binding energy peaks. It seems clear that this will only be possible with a combination of techniques, including modeling of binding energies, vibrational absorption modes, and other structural and electronic data.

1.7 Nanotube curvature, helicity, cross-linking and defect interaction

Although nitrogen dopants modify nanotube behaviour, the behaviour of the dopants themselves will be strongly influenced in return by the physical and electronic nature of the surrounding carbon lattice. In carbon nanotubes this is defined broadly by four categories: nanotube curvature, nanotube helicity, inter-tube or inter-wall interactions, and intra-tube interaction with other dopant atoms.

1.7.1 Nanotube Curvature

In many cases nitrogen doped multi-walled nanotubes exhibit significantly higher tube wall buckling and corrugation than equivalent undoped nanotubes. In addition, nitrogen doped MWNTs always exhibit internal 'bamboo' walls. There are various reasons to expect nitrogen may prefer regions of curvature in nanotubes, and may indeed induce them.

Unlike carbon, nitrogen can adopt stable pyramidal bonding configurations as in the molecule NH_3, where its two remaining valence electrons occupy a shared sp^3 orbital.

It is thus to be expected that nitrogen will be more stable than carbon in regions of high curvature such as folds or kinks. Calculations of Miyamoto *et al.* of graphite sheets at different curvature found nitrogen substitution helped stabilise the curved sheets [128].

In addition semi-empirical Hartree-Fock calculations showed that nitrogen substitution in a graphitic lattice lowers pentagon formation energies, and thus could encourage pentagon formation and therefore induce curvature.

Higher curvature will also stabilise NV complexes, since the tube curvature both aids the out-of-plane displacement of the nitrogen atom and facilitates the formation of a reconstructed carbon-carbon bond between the two carbon neighbours of the vacancy. Note that curvature will also impose a preferential orientation on various defects such as NV and interstitial N, with reconstructed (broken) C-C bonds lying circumferentially in order to minimise (maximise) their length [43].

1.7.2 Inter-Tube and Inter-Wall Bonding

Nitrogen concentration strongly affects the ratio of sp^2 to sp^3 carbon bonds in CN_x thin films. EELS studies of N doped MWNTs shows less sp^2 character of the carbon *K*-edge on the internal nanotube walls where nitrogen concentration is higher [55]. If nitrogen induces sp^3-bonding then this implies either inter-tube or inter-wall cross-linking covalent bonds. Cross-linking is more likely in semiconducting tubes, where substitutional N donor states are localised and so chemically active [67].

Nevidomskyy *et al.* [67] examined C-C bonding between two semiconducting nanotubes, each with a single substitutional nitrogen. A C-C bond forms between the tubes, linking C atoms lying on opposite sides of the hexagon from the substitutional N along the nanotube axis. These sites are where the spin density for the isolated tubes is a maximum. Notably they found such bonding only occurred spontaneously for N densities of at least one bond per two unit cells (8.4 Å). This corresponds to a nitrogen concentration of 1.6%, with nitrogen occupying 25% of sites neighbouring the other tube. Graphite sheet modelling also shows that carbon next to substitutional nitrogen can go sp^3-coordinated [129].

Note that total nitrogen content is not the key factor for cross-linking, but nitrogen content in the area of overlap between graphitic systems. Thus in principle, lower total nitrogen content is required for cross-linking in nanotubes than in flat sheets. By extension, nitrogen induced cross-linking is more likely in buckled, curved and deformed systems. At the extreme end of this spectrum are the azo-fullerenes where cross-linking is seen between two $C_{59}N$ molecules with 1.7% total nitrogen concentration, but where 50% of adjacent sites are nitrogen substituted [28]. In nitrogen substituted graphene sheets, semi-empirical calculations found a flat to buckled transition at [N] of 20% [85]. This transition from graphitic to buckled occurs when the energy gained from maintaining an increasingly disrupted aromatic graphitic bonding arrangement drops below that gained from forming localised sp^3 inter-sheet bonds.

1.7.3 Intra-tube defect interaction

Lammert *et al.* [69] refer to realistically doped tubes with a genuinely random distribution of dopants. However there has not yet been any systematic study of dopant-dopant interactions, and it may well be that there are thermodynamic driving forces for defect superlattices [130], or localized high nitrogen islands such as proposed for boron [131]. Indeed, spatially resolved EELS studies of nickel catalysed nitrogen doped MWNTs shows what appear to be higher nitrogen content (<13 at%) domains within the tubes of ~1-5 nm in size [55].

DFT calculations on (5,5) nanotubes suggest that for these extremely small radius nanotubes it is energetically favourable for nitrogen atoms to lie in neighbouring circumferential sites, since the N-N bond can break, relieving the high curvature strain [98]. However such an effect is unlikely to occur in larger radius tubes. For (10,0) tubes the same group find N-N repulsion. Other groups find next neighbour N in (5,5) tubes to be repulsive due to the retention of the N-N bond distance [94].

1.8 Nitrogen-CNT Surface Chemistry

Nitrogen doped CNTs appear significantly more reactive than their undoped counterparts. Nitrogen doped tubes start to gasify at 370°C, as compared to pure CNTs which burn at 450°C, with oxidative tube destruction primarily occurring at around 540°C (600°C) for doped (undoped) tubes [7]. Nitrogen doped single walled nanotubes (N-SWNTs) were also observed to break more easily under the electron beam in TEM and STEM analysis than pure carbon nanotubes [1]. Finally doped tubes disperse in various solvents not possible with undoped tubes [16].

Fluorination of carbon nanotubes is of interest both as a way to activate the tube surfaces and to increase their solubility in a variety of solvents [132]. Low temperature fluorination of N-doped MWNTs was achieved using BrF_3 vapour [133]. Large diameter tubes were more easily broken into separate compartments and showed higher reactivity, with fluorine penetration through most of the tube layers. The outer layers showed expanded lattice constants (~4.2 Å). This is in contrast to undoped tubes which only show fluorination of the outer walls (also the case in small diameter fluorinated N-CNTs). Interestingly their XPS studies show two N(1s) peaks at 399 and 401.2 eV before fluorination. However after fluorination the first peak disappears, replaced by a peak at ~400.3 eV, interpreted as a conversion of pyridinic nitrogen through fluorination into pyrrolic nitrogen. It suggests the reactivity of nitrogen in doped tubes depends on its configuration. This work shows great promise for gas reactivity of N-CNTs, and this is a subject which needs further study.

There have been various studies of bonding to N-CNTs after acid treatment with H_2SO_4-HNO_3, creating surface –OOH groups. These have then been either activated allowing protein attachment to the tube walls [15] or electrostatically bonded to a surface coating of cationic polyelectrolyte; this was then used to attach gold clusters to the nanotube [134]. It is suggested that acid treatment functionalises the nitrogen defects although comparison with undoped tubes or XPS studies would be needed to confirm this.

Modelling of N_3V defect sites on (5,5) nanotubes shows strong binding of NH_3 (via NH_2 and H) and OH [135], significantly modifying the density of states at the Fermi level. The authors show that OH binds preferentially to C atoms neighbouring the

nitrogen, showing that nitrogen doping chemically activates surrounding carbon atoms in the tube.

A change in the surface reactivity of nitrogen doped nanotubes should be expected, especially for SWNTs. For MWNTs it will be more a question of the synthesis process used, since this determines where the nitrogen is predominantly incorporated into the tube. For example, a high nitrogen concentration in the inner nanotube walls should not have a significant effect on the surface reactivity.

1.9 Electronic transport in nitrogen-doped nanotubes

1.9.1 Electronic transport in undoped carbon nanotubes

In this paragraph concepts of electronic transport in undoped nanotubes are introduced to form a base for discussing electronic transport in nitrogen-doped nanotubes. Electrical transport in undoped carbon nanotubes (CNTs) has been intensively investigated. Conduction in CNTs occurs via the delocalized π-electron system [136].

At room temperature, both, metallic and semiconducting SWNTs (without external gate) are ballistic conductors with two and one spin degenerate conducting channel(s), respectively [137-139]. The channels belong to the first π- and π^*-band of the delocalized π-electron system.

Involving higher bands for transport than the first π- and π^*-band would require a massive electron-excitation energy of the order of 1 eV corresponding to a temperature of about 1200 K [140]. Thus, at ambient conditions, without external excitation (e.g. incident light, electric field), SWNTs only have two spin-degenerate conducting channels available for charge transport. Each of these channels can carry the conductance quanta $G_0 = 2e^2/h$ (e: electron charge, h: Planck quantum) [141].

The energy gap between conduction and valence band in semiconducting SWNTs scales inversely with the nanotube diameter (typically around 0.5 eV for a 1 nm diameter tube) [141].

Ballistic conduction of charge carriers in SWNTs occurs mainly because of the absence of efficient electron-phonon interactions and weak scattering cross-sections for defects in the hexagonal lattice (e.g. pentagon-heptagon defects). Indeed femto-second time-resolved photoemission measurements have shown that the mean free path of metallic SWNTs is of the order of several μm [142]. This extraordinary long mean free path is well above the typical lengths of SWNT based electronic devices with conducting channel lengths in the sub-micron regime. Thus, SWNTs can be regarded as excellent candidates for low-power consumption molecular electronic building blocks.

With decreasing temperature electron-electron interactions become more important within the SWNTs. This is a consequence of their high electronic 1D character, which leads to an effective increase of the Coulomb interaction between the electrons in the nanotube. The electron-electron interactions shift the electronic state of the SWNTs from a ballistically conducting Fermi-liquid to a correlated 1D electronic system. This state can be described by the Tomonaga-Luttinger formalism. In contrast to a Fermi-liquid, a Tomanaga-Luttinger liquid is characterised by collective charge and spin-excitations [143-145]. In this state the conductance at source-drain voltages much smaller than the thermal energy (also called zero-bias conductance) follows a power-law dependence in the temperature.

MWNTs consist of a concentric arrangement of different diameter SWNTs (similar to a Russian doll) which can be either metallic or semiconducting and are of different helicity. The outer SWNT can have a diameter of several tens of nanometres. The distance between neighbouring SWNT-shells is approximately the same as the separation found in planar graphite (3.3539 Å). Each of these SWNT-shells is principally a ballistic conductor, thus MWNTs could be expected to be also ballistic conductors at room temperature with mean free paths comparable to SWNTs. However, the intershell interaction destroys the ballistic conduction properties of each SWNT shell. Pictorially, an electron wave propagating on a SWNT shell has certain

probability to be scattered into a neighbouring shell [146]. From a more theoretical point of view this interaction may be described by an Anderson-type of disorder (random modulations of the nanotube lattice atom potential, but constant in time) in each of the shells [147]. In particular, additional disorder is introduced in each SWNT shell due to incommensurability effects of the different helicities of the neighbouring shells [148]. Experimentally, the intershell interaction leads to the observation of fractions of the conductance quanta G_0 [149]. As a consequence the mean free path of MWNTs at room temperature is considerably shorter than in SWNTs, exceeding at best not more than one to two μm.

Due to the intershell interaction and the fairly large outer diameter, MWNTs exhibit a much weaker 1D character than SWNTs. In fact magnetotransport experiments indicate strongly that MWNTs have rather to be regarded as 2D electronic systems [150]. The cross-sections for electron-defect scattering is suggested to be significantly larger than in SWNTs.

Towards low temperatures, temperature-dependent measurements of the zero-bias conductance in MWNTs have shown also a power-law dependence similar to that of SWNTs [151, 152]. Initially this power-law dependence was interpreted to be a finger-print of the existence of a Tomonaga-Luttinger-liquid state in MWNTs. However, the experimentally observed existence of non-negligible disorder in MWNTs suggests another scenario, since for the development a Tomonaga-Luttinger-liquid state a well-established ballistic conductance is a necessary pre-condition. This pre-condition is less and less fulfilled for MWNTs with increasing number of tube shells and diameter. In the row of these discrepancies several theoretical models have been developed with different type of disorder origin in MWNTs [148, 153, 154]. However, all of them introduced only time- and temperature-independent disorder. Concerning the zero-bias conductance, Mishchenko *et al*. developed a theory describing a MWNT as disordered nano-wire with electron-electron interactions and constant relaxation times [154]. The theory provides expressions for the zero-bias conductance for weak and strong disorder degrees. In the limit of weak disorder the power-law dependence of the zero-bias conductance is reproduced, whereas for strong disorder a more complex exponential expression is found. Indeed, zero-bias

conductance measurements versus temperature on boron-doped MWNTs showed satisfactory matching with this theory [155][.

1.9.2 Theories on transport in substitutionally doped carbon nanotubes

Electronic density of states of nitrogen doped carbon nanotubes

The substitution of carbon atoms in the honeycomb lattice of a CNT by atoms with a different number of valence electrons will in general introduce additional states in the density of states (DOS) of the CNT. Whether these will be electron-donor or electron-acceptor state or none of these two, depends crucially on the way the hetero atoms are substituted into the lattice. That is, in a graphite-like way or differently (e.g. pyridine-like way) as discussed previously. In the following, we will focus on the electronics most relevant case of graphite-like substitution of nitrogen atoms into the carbon lattice of a SWNT.

Consider first the substitution of a carbon by a nitrogen atom in a graphite-like way into the CNT lattice of a metallic SWNT. Since nitrogen is 5-valenced and carbon has four valence electrons, the nitrogen state will be located above the Fermi-energy of the undoped SWNT as depicted schematically in Figure 14a. For a SWNT with a diameter of about one nm the nitrogen states will be found approximately a few hundred meV below the first van Hove singularity of the π^*-band [98, 100]. The exact position of the nitrogen states depends on diameter, helicity, and number of nitrogen atoms incorporated.

If the incorporated nitrogen ionizes, that is, liberates its excess electron to the π-electron system of the SWNT host, the Fermi-energy will shift upwards in energy relative to its initial position (see Figure 14a).

In Figure 14b the case of a DOS of a semiconducting SWNT with a graphite-like incorporated nitrogen is shown. Similar to the metallic SWNT the nitrogen states are found above the initial position (in the centre of the energy gap) of the Fermi-energy. The nitrogen states lie about 150 to 200 meV below the conduction band of a nanotube with a diameter of one nm, depending on the tube helicity and the number of nitrogen atoms.

As the nitrogen states ionize, the liberated electrons will occupy empty states at the edge of the valence-band of the tube and an *n*-type semiconducting SWNT is created. Charge transport occurs solely through the π^*-band channel. The Fermi-energy of the nanotube will shift (relatively) upwards in energy and positions at the nitrogen states in the DOS (see Figure 14b).
It has to be noted that the above descriptions and considerations hold exclusively for graphite-like substitution of carbon by nitrogen atoms. If the substitution is for example in a pyridine-like way and/or accompanied by a structural defect in the carbon honeycomb lattice, it is *a priori* not clear if additional states in the π-electron DOS will be created, and if so if these will be acceptors or donors.

Finally it has to be remarked that the ionization of dopant states in CNTs is not a trivial task. For ionization the ionized dopant atom has to be electrostatically screened by the surrounding electron sea to conserve charge neutrality. Since SWNTs have a strong electric 1D character, their screening properties are rather poor [156], which is in particular the case for semiconducting nanotubes. For a 1D doped semiconductor (assuming Gaussian statistics), dopant charges giving rise to extremely short ranged Coulomb fluctuations unlike in bulk materials. Thus screening, a longer range effect, is ineffective. Notably, calculations show that the potential fluctuations are independent of tube radius for a fixed dopant concentration [69].
The problem of electrostatic screening is considerably reduced in MWNTs due to their larger diameter and the existence of neighbouring SWNT-shells, that is, because they are rather 2D than 1D electronic systems.

1.9.3 Short overview on the charge transport theories in undoped, disordered and substitutionally doped carbon nanotubes

Undoped carbon nanotubes
As discussed previously SWNTs are ballistic conductors at ambient conditions. Ballistic conduction can be described within the framework of the Landauer-Büttiker-formalism [157, 158]. In a ballistic conductor the electrons do not suffer from any scattering. The situation is analogous to electromagnetic waves in a wave-guide. In the latter a certain number of transverse modes can propagate the wave-guide depending on the actual shape of the wave-guide. In the case of electrical transport the

number of transverse modes, that is, the contributing bands (c.f. previous section), originate mainly from the confinement of the electrons in the conductor. In the case of CNTs the confinement is given by the translational symmetry along its circumference.

Thus, the total conductance G is proportional to the number of bands available in the ballistic conductor at the Fermi-level times G_0. The conductance quantum $G_0 \approx 19.4$ μS naturally occurs within the Landauer-Büttiker formalism (the reader is referred to the vast literature on this topic). However, the conclusion that the total conductance is given by G_0 times the number of available bands is only valid for perfect transmission of an incident electron wave-function from an electron reservoir (electrical contact/electrode) into the ballistic conductor. In the case that there is a finite probability of the wave-function to be reflected from the conductor/reservoir interface, G is given by the sum over all transmission coefficients T_i. T_i gives the probability that an electron from the reservoir enters in the band i of the conductor. Thus, for a metallic SWNT contacted to two electrodes with the Fermi-level at the charge-neutrality-point

$$G = G_0(T_1 + T_2)$$

It is to be stressed, that $(G_0 \cdot (T_1 + T_2))^{-1}$ is the contact resistance of the SWNT connected to two reservoirs. It is sometimes misleadingly called the resistance of the SWNT. If the transmission is perfect then a metallic SWNT has the total conductance $G \approx 9.7$ μS corresponding to a resistance of about 6.4 kΩ (Fermi-level at the charge-neutrality-point). It should be noted that the transmission coefficient is a function of the Fermi-energy position and varies stepwise with this position, reflecting the density of state of the carbon nanotube.

The confinement in a CNT leads to a strong electronic 1D character of the SWNTs and is also responsible for its ballistic conduction properties. This pronounced 1D character of the electronic system has severe consequences at temperatures (well) below room-temperature. In this temperature regime electron-electron interactions come to play and the Fermi-liquid picture, that is, the single quasi-particle picture breaks down. For illustration consider a perfect 1D system of free electrons consisting

of a linear chain of length L of equidistant atoms, each of them contributing one electron. In this case the reciprocal space of the linear chain consists also of a linear chain where the Fermi-surface is reduced to two Fermi-points $+k_F$ and $-k_F$. This 1D-topology leads to a considerable difference in the response of the free electron gas to any kind of external perturbation, compared to 2D or 3D electron systems [159].

Consider now an external, time-independent potential $\varphi(x)$ acting on the 1D free electron gas and let $\varphi(q)$ be its Fourier-transform [159]. The perturbing potential leads to a rearrangement of the electron density which may be described by an induced charge density $\rho_{ind}(x)$. The Fourier transform of the induced charge density $\rho_{ind}(q)$ and $\varphi(q)$ are connected through the so-called Lindhard-response function $\chi(q, T)$ with $\rho_{ind}(q) = \chi(q, T) \cdot \varphi(q)$ [159]. $\chi(q, T)$ can be determined for wave-vectors q close to $2k_F$ by assuming a linear dispersion relation around the Fermi-energy E_F, $(E(k) - E_F) \sim v_F \cdot (k - k_F)$ [159]. This leads to the expression for the Lindhard-function proportional to $ln|(q+2k_F)/(q-2k_F)|$. Thus, for $q = 2k_F$, $\chi(q, T)$ has a logarithmic divergence which is due to the particular topology of 1D electronic systems. The most significant contribution to the divergence arises from pairs of states, one occupied, the other unoccupied, which are $2\ k_F$ apart from each other [159].

In contrast, in higher dimensions the relative amount of these kinds of states is significantly reduced such that the singularity vanishes. The behaviour of the response-function has important consequences: an external perturbation leads to divergent charge redistributions of the 1D electron system [159] and at $T = 0$ K the electron gas is unstable with respect to the formation of a periodically varying electron charge density (long-range interaction) [159]. In consequence, such a 1D electron system cannot form a stable Fermi liquid as it is known for 3D or 2D metals since the interaction cannot be “hidden” in the effective mass of fermionic single particles. Further, instead of single particle excitations, only collective excitations are possible [159].

Since the single particle breaks down in 1D electronic systems, the electron system shifts to a correlated state. Depending on the particular properties of the atomic lattice potential either so-called charge- and spin-density wave systems or a Tomonaga-Luttinger-liquid state can develop. A detailed description of all these is beyond the scope of the present overview and the reader is kindly referred to the existing vast and rich literature [143-145].

For the case of SWNTs only the essential and relevant results will be stated here. The zero-bias conductance for SWNTs follows a power-law dependence in temperature,

$$G_{zero\text{-}bias}(T) \sim T^{\gamma},$$

where γ is a measure for the electron-electron interaction strength. In case, the applied voltage V to the SWNT exceeds the thermal energy of the environment of the nanotube the conductance follows the power law:

$$G(V) \sim V^{\gamma}$$

Both power-law dependencies arise from the fact that the density of states of the collective excitations in a Tomonaga-Luttinger liquid follows a power-law dependence, $n(E) \sim E^{\gamma}$, where E is the energy of the excitation [140]. Indeed, Bockrath *et al*. [160] have experimentally demonstrated the existence of a Tomonaga-Luttinger-liquid state in SWNTs by measuring the conductance of individual metallic SWNts in a two-point configuration.

The question of the existence of Tomonaga-Luttinger-liquids in MWNTs will be addressed below.

Disorder in carbon nanotubes

In the previous section the ballistic nature of the charge transport in SWNTs was discussed. Since ballistic conduction implies the absence of disorder, theories on disordered CNTs mainly address MWNTs [146, 148, 154]. However, the unit cell of CNTs can be fairly large, that is contain a large number of atoms [136] and thus the theoretical calculations are mainly restricted to "high symmetry" armchair and zig-zag and small diameter (only a few nm or even less) CNTs due to lack of computational power. For example a (10,10) nanotube has a 40-atom unit cell and a (12,0) unit cell contains 48 atoms, whereas a (10,7) has 143 atoms in the unit cell.

For the same computational power reason theories normally assume, apart from a very few exceptions (e.g. Ref. [146]), that charges in MWNTs are exclusively propagated by the outer SWNT-shell. These limits of theoretical techniques are often forgotten when comparison to experimental results are made, and misleading conclusions may be derived. Therefore, special care has to be taken in this point.

It is noteworthy to stress that the theories, though being nominally developed for MWNTs, are also applicable to SWNTs, because of the assumption that only the outer shell carries a current, and other shells are only there to introduce disorder.
In the following two central carbon nanotube specific theoretical approaches will be sketched and finally the problem of the Tomonaga-Luttinger-liquid state in MWNTs briefly discussed.

MWNTs consist of concentric SWNT-shells. Even under the assumptions that each of these shells is free of defects, the intershell interaction will modulate the atomic potential of each shell, that is, introduce time- and temperature independent disorder. Roche *et al*. developed a theoretical description of the quantum diffusion of electronic wave-packages as function of time on double- and triple-walled carbon nanotubes taking the interaction between two SWNT shells with commensurate and incommensurate pair of indices (or helicities) into account [148]. For example, the zig-zag tubes (7,0) and (14,0) show commensurate helicities, whereas a (10,4) nanotube is incommensurate in helicity with respect to a (6,6) SWNT. However, the theory excludes potential scattering from one shell to another.
The quantum diffusion with time is described within this theory by the time t dependent diffusion constant $D_\psi(t)$. In Figure 15 the calculation results for the commensurate and incommensurate double-walled nanotube (9,0)@(18,0) and (9,0)@(10,10), respectively, and an incommensurate triple-walled nanotube are shown [148].

The calculation results in Figure 15 reveal that in the commensurate case the wave-package diffuses linearly in time with a constant (average) velocity along the outer shell of the double-walled CNT. That is, the electronic wave-package travels in a ballistic way. In contrast, in the two incommensurate cases $D_\psi(t)$ changes with time indicating a varying average velocity with time. This is the fingerprint of diffusive transport, that is, scattering of the electronic wave-package. In conclusion it can be stated that incommensurable SWNT-shells in MWNTs lead to a diffusive conduction mechanism along the MWNT.
The theory further allows to predict a length L dependence for the total conductance $G(L)$ of the MWNT, $G(L) \sim L^{(\eta-1)/\eta}$, where the parameter η is a measure for whether

the conduction is ballistic (η = 1) or diffusive (η = 0.5) due to incommensurability effects [148]. Indeed the theory has been confirmed by measurements on single, boron-doped MWNTs [154]. It has to be noted that the theory treats conduction in MWNTs in a quasi-particle picture (Fermi-liquid) and does not take electron-electron interactions into account, that is, a possible electronic 1D character of the system.

The consideration of electron-electron interactions versus disorder has been subject of a theoretical work of Mishchenko *et al*. [154]. In this work a MWNT is modelled as a disordered quantum wire with N conducting channels with including electron-electron interaction strength and describing disorder by a constant relaxation time for the electrons. Interestingly, the theory does not make any specific assumptions on the origin of the disorder.

On one hand, the theory can reproduce the main feature of the Tomonaga-Luttinger liquid in the limit of zero temperature. That is, the density of states $n(E)$ of the collective excitations (E: energy) of the correlated electron state in the nanowire follows a power-law dependence, $n(E) \sim E^{\gamma}$ if the Fermi-energy of the system is larger than the effective disorder potential.

On the other hand, in case the effective disorder potential becomes larger than the Fermi-energy of the system, the electron system in the disordered wire with electron-electron interactions can not be any more in a Tomonaga-Luttinger-liquid state. Instead, the density of states $n(E,T)$ of the excitations follows an exponential dependence on energy and temperature. The excitations are still to be regarded as collective excitations (low-energy plasmons), however, with a wavelength smaller than the length of the nanowire. Noteworthy, the theory implies that in a disordered quantum nanowire a crossover from a Tomonaga-Luttinger-liquid state to a disordered state can occur while changing the Fermi-energy and/or the temperature of the system. Also the theory is applicable to metallic SWNTs containing disorder by setting the number of conducting channels to four.

Carbon nanotubes doped by substitutional nitrogen

Nitrogen is the natural choice for doping CNTs since it differs only by one additional valence electron from a carbon atom. Thus, a relatively easy incorporation into the carbon honeycomb lattice should be achievable. Indeed, the nitrogen atom, substituted in a graphite-like way was calculated to differ only by 0.01 Å from the equilibrium position of a carbon atom [67]. However, it is not immediately evident that nitrogen doping will lead to improved conductance due to new sources of electron backscattering [161, 162]. Indeed theoretical calculations predict that electron backscattering is possible by quasibound states due to the nitrogen doping [162].

An approach based on tight binding methods correlated to *ab-initio* calculations to describe the electronic transport properties of nitrogen- and boron-doped (graphite-like way) has been performed by Latil *et al*. [163]. This method principally allows for the calculation of relevant transport properties such as the mean free path or conductance scaling for varying concentrations of boron and nitrogen atoms. Pictorially speaking, the approach puts at zero temperature an electronic wave-package on the doped SWNT atomic honeycomb lattice and correlates the time the wave-package needs to diffuse, τ_D, over a chosen length, L_D, along the nanotube with a total length larger or equal to L_D. The main result of this approach is an expression for the conductance (derived from the Kubo formula) which links L_D with the electronic density of states per unit length in the tube, $\rho(E)$, and the diffusion coefficient $D(\tau_D)$,

$$G_0(E, L_D) = 2e^2 \cdot \rho(E) \cdot (D(\tau_D)/L_D)$$

where E is the Fermi-energy position and e the electron charge [163].

The calculated results for the conductance of 0.1 atom% nitrogen- and boron-doped, metallic nanotubes as a function of Fermi-energy position and different lengths L_D are depicted in Figure 16 [163]. Nicely, the symmetrical action of nitrogen and boron dopants on the conductance is apparent.

It has to be noted at this point that the presented theory does not account for the electronic 1D character of a SWNT. That is, electron correlation has not been taken into account and transport is described in a quasi-particle picture.

Within this context it is interesting to address the spatial variation in dopant density of 1D systems. The dopant density is more important in 1D systems than in bulk semiconductors, since electrons cannot easily bypass anomalous regions [69]. However this may also prove an advantage since the interfaces of such regions act as *p-n* junctions, suggesting a way to produce chains of *p-n* junctions along a nanotube ("diodium") [69]. In calculations with random defect distributions in (8,0) semiconducting tube, it was found that nitrogen rich regions can reduce the local density of states, which in a 1D structure may be enough to block charge transport [69]. Heterogenous defect distribution with high doping levels (~1%) leads to regions with strong non-linear behaviour, which may end at low enough temperatures into quantum-dot- / junction-structures. Calculations on small amounts of random disorder showed a drop in current of ~10% compared to non-disordered systems [164]. For *periodically* spaced single nitrogen dopants, transport in semiconducting tubes is calculated to become metallic with a negative differential resistance. This is explained through current carrying defect bands being brought into alignment through the applied bias voltage and later going out of alignment at higher applied bias voltage [164].

Also, the introduction of nitrogen atoms is theoretically predicted to give rise to chiral current flow along the nanotube due to symmetry breaking [165, 166]. However, this theoretical considerations and predictions are undermined by recent experimental investigations where chiral currents have been observed in undoped single-walled carbon nanotubes [167].

Experiments on the charge transport on carbon nanotubes doped by substitutional nitrogen

The vast majority of reports on doped CNTs address CNTs which are doped after synthesis, either by exposure to different gases or in electrolytic liquids. This type of post-doping primarily is a gating effect, that is, the electrostatic environment of the CNTs changes and therefore the CNT's Fermi-energy shifts. In particular, this type of doping does not introduce a specifically high disorder to CNTs, otherwise for example no ballistic conduction at ambient conditions or the fingerprints of the Tomonaga-Luttinger-liquid state could have been experimentally observed in CNTs. In how far electronic doping though chemical functionalization, that is, the addition of side-groups to the carbon lattice, is successful is a topic on debate. No sufficient experimental charge transport data are reported in literature on chemically functionalized nanotubes.

Although quite some advances have been made in the (recent) past [1, 168-170] on the *in-situ* synthesis doping of SWNTs and MWNTs through substitution of carbon by nitrogen atoms, only a very limited number of electronic transport data is so far found in the literature.

In the previous sections the principal differences between charge transport in MWNTs and SWNTs have been already stressed. One of the main differences is the circumstance that SWNTs have no constitutionally occurring source of disorder (no intershell interaction). Also, the experimental observation of ballistic transport in SWNTs [137-139] at room temperature indicates that lattice defects have a relatively small scattering potential.
Therefore, the question arises of what strength the disorder potential would be due to the substitution of carbon by nitrogen atoms in a SWNT. To tackle this question, the zero-bias conductance is the best charge transport measure to detect disorder influences of the substitional nitrogen dopants in a SWNT.

For nitrogen-doped MWNTs and SWNTs only a small amount of experimental (direct) electrical transport data are reported. The vast majority of the literature on transport in nitrogen-doped CNTs concerns theory.

Choi *et al*. reported one of the first electrical transport and thermopower measurements on mats of nitrogen- and boron-doped MWNTs [171]. The morphology of the boron-doped MWNTs was well-graphitised, that is, the MWNT consisted of SWNT shells. In contrast the nitrogen-doped MWNTs showed bamboo-like features, but concentric shells of SWNTs were still apparent [171].

The thermopower measurements revealed that the majority charge carriers in nitrogen-doped MWNTs are electrons. That is, an *n*-type-conduction is principally achievable in MWNTs via substitutional doping. In Figure 17 the resistance of the mats as a function of temperature is shown [171].

The resistance in the doped MWNT mats increases only slightly relative to the undoped MWNT mat with decreasing temperature. The plot in the inset indicates that the charge transport through the mats is dominated by a hopping mechanism. The results are understood, taking into account that in mats or networks of nanotubes, the main barrier for the charges is not within the tubes, but is the hopping from one tube to another. Notably, the doping of MWNTs by substitution with nitrogen and boron reduces the inter-tube hopping barrier.

One of the first reports on the application of nitrogen-doped MWNTs for field-effect transistors was reported by Xiao *et al*. [172]. They fabricated a field-transistor using an individual nitrogen-doped MWNT and could show that the device acts as an *n*-type transistor. However, the MWNTs used in their experiments where rather large in diameter (around 50 nm) and were not well-graphitised [172]. That is, the MWNTs consisted mainly of a chain- and bamboo-like structure, and almost no concentric SWNT-shells were observed [172]. Thus, although an *n*-type conduction could be achieved, no reliable conclusions on the influence of nitrogen-doping of well-graphitised MWNTs can be drawn.

Nitrogen atoms substituted in the nanotube honeycomb lattice differ only slightly in size from the carbon atoms [67]. Therefore, only a relatively small lattice strain is apparent, and thus no significant enhancement of the nitrogen scattering cross-section

is to be expected. As a consequence electrical transport for charge carriers being energetically well separated from the nitrogen dopant levels in the π^*-band should not suffer from scattering.

To test this hypothesis the most suitable way is to measure the temperature-dependence of the zero-bias conductance of a nitrogen-doped, metallic SWNT in its *p*-conducting state. That is, the Fermi-energy lies within the π-band. In Figure 18 the zero-bias conductance of a nitrogen-doped SWNT, with 1 atom% dopants, under these conditions is shown [173]. The plot is in double-logarithmic representation. The dotted line corresponds to power-law dependence, fingerprint of a Tomonaga-Luttinger-liquid state. Obviously, the data points deviate from this dotted line. The data are better fit by the dashed dotted line. This line corresponds to a fit based on a disordered nanowire [154] with *N* conducting channels in case the Fermi-energy is smaller than the effective disorder potential (c.f. to the discussion previously). This experimental result is surprising since it is not necessarily expected by the theoretical considerations (c.f. to the previous sections). A possible solution would be to take into account a more long-ranged interaction between the nitrogen dopant atoms and the current carrying charges. Indeed, electron-energy-loss results showed the existence of differently substituted nitrogen atoms, graphite- and pyridine-like [168]. The pyridine-like nitrogen is expected to have a permanent electric dipole moment which acts as additional scattering mechanism for the current carrying electrons [173]. In fact the fit representing the dashed dotted line in Figure 18 takes this electrical dipole interaction into account [173].

The experiments on the nitrogen-doped MWNTs demonstrated that these types of CNTs exhibit relatively strong disorder already at room temperature and as a consequence any notable ballistic conductance at room temperature is suppressed. However, the situation turns out to be different for nitrogen-doped SWNTs. Electrical transport measurements on individual nitrogen-doped metallic SWNTs have shown that even at room-temperature ballistic conductance over lengths over several hundred nm is possible even with 1 atom% of dopants [173].

The interest in nitrogen-doped CNTs in terms of application is the control of the type of charge carriers within the carbon nanotubes. This control is one key-issue for a

successful implementation of CNTs in nano- and molecular-electronics. Another key-issue is the power-consumption of a potential device (e.g. field effect transistor) based on doped CNTs.

For doped MWNTs, control on *n*- and *p*-type conduction seems to be achieved. However, doped MWNTs show a high degree of disorder which has two important consequences. The increased scattering of charge carriers increases the power consumption of the device and at the same time increases Joule heating. The latter is in particular of importance because it can lead to device malfunction and in the worst case to failure in a comparably hot environment (e.g., CPU or VIA in integrated circuits).

In contrast, nitrogen-doped SWNTs still exhibit ballistic conduction at ambient temperature over several hundred nm. Thus, the power-consumption and the risk of malfunction of devices based on doped SWNTs are significantly reduced compared to doped MWNTs. But SWNTs are more sensitive to the environment (gases) due to their 1D molecular character and suffer from a higher work-function mismatch with typical electrical contact materials like gold or copper. In particular the latter may impede the creation of *n*-type-conduction due to electron extraction from the nanotube.

1.10 Applications

Nitrogen doped CNTs have a range of potential applications utilising their physical and chemical differences from conventional undoped tubes. In the following section we summarise recent investigations of nitrogen doped CNT use for field emission, sensors, metal storage and composites. Their use in nanoelectronics, although promising given their unusual transport characteristics detailed above, is currently only theoretical. They may also have useful application in photonics [174].

1.10.1 Field Emission

Carbon nanotubes have attracted great interest as field emission sources. For a recent thorough review on field emission in doped nanotubes see Zhou and Duan [175]. Their aspect ratio promises extremely high field enhancements (enhancement factor, $\beta=h/r$, where h is the tip height and r is the radius of curvature at the tip [176]. In practise the nanotube spacing is crucially important since too high packing densities lead to a smearing of the potential gradient around the tips and a reduction of β. Nanotubes are relatively chemically inert which reduces the conventional requirement for high vacuum operating environment [177].

It might be expected that nitrogen-doped CNTs would be good candidates for field emission devices, due to the additional donor states just above the Fermi level. For this reason there have been various attempts to measure field emission characteristic of isolated and bundled nitrogen-doped CNTs.

Kurt *et al* examine field emission from decorated large radius tubes, and find a strong radius dependence with best emission from their smallest radius tubes [178, 179]. Emission properties compare reasonably well with pristine tubes [180]. Wang *et al* find a turn-on field of 1.5V/μm for highly nitrogen doped tubes [111], with current densities of 80μA/cm^2 for fields as low as 2.6V/μm, considerably better than their undoped counterparts. Other groups [54] suggest they may see turn-on fields as low as 0.8V/μm.

More recent work on aligned CN_x nanotubes claim to have high 1.280 mA/cm^2 current densities for 2.54V/μm applied fields [181]. N doped MWNT bundles were also shown to be stable field emitters up to very high current densities (~0.4 A/cm^2) [182]. However very large diameter nanotubes with low [N] doping show similar emission properties to equivalent undoped tubes, and in this case incorporated nitrogen seems to play little, if any, role in field emission [183].

It is suggested that N-doped MWNTs should be improved electron emitters due to their bamboo or 'nanobell' morphology, with the thin walled MWNTs being able to emit along the edge of the bamboo ridges [184], although these may be too densely packed to contribute significantly [183]. In addition the catalyst particles tend to lie at the base of the nanotubes and so do not interfere in the emission process [181]. Open or closed tube tips will also significantly alter field emission properties [185], and if N terminated open tube tips can be realised [105] this should lead to significantly enhanced field emission properties.

Electron emission studies from individual N doped MWNTs found a work function of 5.0eV [186], similar to that of undoped MWNTs [187]. However in bundled samples using ultraviolet photoelectron spectroscopy, the work function was shown to be lower than that of undoped nanotubes [184].

Density functional calculations of SWNT tips with substitutional nitrogen show the nitrogen related donor levels reduce the work function of the tip and significantly enhance the localised density of states [188].

Nitrogen doping can also sensitise nanotubes for gas absorption, which may suggest another way to improve field emission properties of N doped nanotubes. Indeed this effect may be responsible for some of the low emission voltages observed. It therefore remains an open question of whether N doped CNTs will open the way for nanotube based field emission devices.

1.10.2 Gas Sensors

N-CNTs should show significant advantages over undoped nanotubes for gas sensor applications, both due to their reactive tube surfaces, and the sensitivity of their transport characteristics to the presence, distribution and chemistry of nitrogen (see Transport section above). Peng and Cho first suggested N-CNT for use in gas sensors, due to the ability of nitrogen dopants to bind to incoming gas species [189].

Villalpando-Páez *et al.* [135] investigated the conductivity of N-CNT films and compressed pellets with various gases (NH_3) and solvents vapours (ethanol, acetone, chloroform, gasoline, pyridine, benzene). Both chemisorption (permanent conductance change) and physisorption (transient conductance change) was observed, depending on the species. The films showed high sensitivities and response times (0.1-1 s).

1.10.3 Metal Storage/Metal adsorption

The modulated, activated surfaces of highly nitrogen doped MWNTs make them in principle interesting candidates for gas and metal storage materials. Notably 'nanobell' style bamboo N-MWNTs show graphite sheet termination on the surface of

the neighbouring bell structure [49], a morphology highly suited to intercalation. Studies of Li storage in N-doped CNTs show efficient reversible storage up to 480 mAh/g, significantly higher than that of undoped tubes, or the theoretical capacity of graphite (372 mAh/g) [190]. It is not clear how the limited ability tubes have to expand their interplanar spacing during intercalation affects storage behaviour. For a recent review on lithium insertion in carbon nanotubes see Ref. [191].

1.10.4 Functionalisation

The nitrogen in the nanotubes can be seen as regular defects which change the chemical behaviour of the tubes. Therefore the reactivity of these nitrogen doped nanotubes can be estimated to be more reactive than un-doped carbon nanotubes of same diameters. Only one single report deals with the changed reactivity and functionalisation of nitrogen-doped SWNTs. Holzinger *et al.* [16] demonstrated that it was possible to functionalise nitrogen doped tubes using a procedure normally utilised for the fullerenes [192] which are significantly more reactive than pristine nanotubes. For all steps in the functionalisation processes it was observed that the nitrogen-doped tubes behaved significantly different to their undoped counter part. Also the tubes were easier to disperse in common solvents.

1.10.5 Composites

Nitrogen doped nanotubes may in find extensive application in composite design, due to their reactive surfaces, allowing increased nanotube-matrix interaction.

There is interest in bonding matrix polymer molecules directly to nanotube surfaces to increase matrix-nanotube adhesion and fibre pull-out energies, and a nitrogen activated nanotube surface facilitates this. Nanotube dispersion in the matrix is important for achieving homogenous composites and therefore improved solubility of

nitrogen-doped tubes should also provide an advantage over undoped nanotubes. This is clearly an area in need of further study.

1.11 Summary and Conclusions

Nitrogen and boron doping of carbon nanotubes is a subject still in its infancy. Many questions concerning dopant configuration and distribution in the nanotubes remain unresolved, and there is much scope for systematic studies of the various synthesis parameters in order to optimise tube growth.

Spectroscopy suggests different types of bonded nitrogen within the tubes, and early studies intriguingly suggest these may be selected based on careful catalyst choice and growth conditions. We are certainly a long way from having spatial control over dopant distribution, a dream for future nanoelectronics applications.

Nitrogen-doped nanotubes demonstrate that doped nanotubes with other hetero atoms such as boron show many properties that are markedly different from their undoped counterparts. This ranges from their physical response to solvents and chemically active surfaces, to their vastly different transport response depending on tube helicity. Once we can learn to precisely control these properties, doping of nanotubes may well prove more scientifically and technically important than their undoped cousins. This will truly be opening the door to the promised nanotechnology revolution, moving from nanotubes as a crude raw material to second generation doped nanotubes with properties which can be customised to end-user specification.

1.12 Acknowledgements

Thanks to Odile Stéphan, Michael Holzinger, Patrick Bernier, Tiberiu Minea, Sylvain Latil, Stephan Roche, Siegmar Roth and Brigette Bouchet for useful discussions. CE acknowledges EU "nano2hybrids" contract NMP3-CT-2006-033311 for funding.

1.13 References

1.14 Figures and Tables

Method	**Nitrogen concentration / nanostructure / references**
Aerosol assisted CVD Acetonitrile / tetrahydrofuran (CH_3CN/C_4H_8O) C/N = 6	~ 20 at% [2]
Pyrolysis of dimethylformamide over an iron catalyst ($HOCN(CH_3)_2$)	2-16% [31]
Pyrolysis of pyridine over a cobalt catalyst (C_5H_5N)	~2% [48]
Pyrolysis of 2-amino-4,6-dichloro-*s*-triazine ($C_3N_3Cl_2NH_2$) over a cobalt catalyst	< 1-2% [193]
CVD of acetylene/ammonia/ferrocene ($C_2H_2/NH_3/Fe(CO)_5$)	3-7 % depending on growth temperature (750-950°C) [14]
microwave plasma enhanced CVD of CH_4/N_2 on Fe particle coated Si or SiO_2 substrates	15-17% [194]
Pyrolysis of nickel phthalocyanine ($NiC_{32}N_8H_{16}$)	[N] not given [30] 0–5% (graphitic layer) [195]
Pyrolysis of iron phthalocyanine ($FeC_{32}N_8H_{16}$)	~10 % [196]
classical CVD acetylene/ammonia mixtures	2-6 % [197]
Pyrolysis of iron phthalocyanine ($FeC_{32}N_8H_{16}$) On a Si substrate	≤ 9% [111]
Pyrolysis of melamine in presence of ferrocene $C_3H_9N_6$ / $Fe(C_5H_5)_2$	10% [29] Inclusion of N_2 gas
Pyrolysis of Melamine over an iron catalyst Pyrolysis of Melamine over a nickel catalyst	4-5 % [55] 3-5 %
Pyrolysis of Melamine over laser-etched Fe substrates	<7% [110]
Aerosol assisted CVD (Jetspray) Benzylamine / Ferrocene $C_6H_5CH_2NH_2$ / $Fe(C_5H_5)_2$	<5% [198]

Pyrolysis of Acetonitrile over a mixed Ni:Co catalyst	[N] depends on Ni:Co ratio: 0:1 (0.70%), 3:7 (0.50%), 1:1 (1.20%), 7:3 (0.60%), 1:0 (1.20%) [33]
Pyrolysis of acetonitrile over a mixed Ni:Fe catalyst	[N] not given [56]
Floating catalyst CVD method ferrocene/pyridine/ NH_3	[N] from 4-10at% Controlled by varying theNH_3 concentration [115]
Pyrolysis of acetonitril over solid solutions of Ni/Co	[N] max 1.2% [N] depends on Ni/Co stochiometry [33]
Pyrolysis of acetonitril over Fe-impregnated zeolites	[N] 6-9 at% Depending on synthesis temperature [199]
CVD synthesis CH_4/NH_3/Ar over a iron-molybdenum catalyst with MgO support	Double walled tubes [N] ~3 at% nitrogen primarily in the inner tube [170]
Pyridine/Ferrocene/NH_3 and Ar	[N] up to 8.8% Depending on NH_3 flow rate and temperature [117]
Pyridine/ferrocene/melamine/H_2	Coiled nanotubes [N] ~3.5% [118]

Table 1. Nitrogen concentration, [N], in MWNTs as a function of nitrogen and carbon precursors synthesised using CVD or CVD-type methods.

Figure 1. Dark-field image of nitrogen doped multi-walled nanotubes.
Copyright Université Paris-Sud, STEM Group.

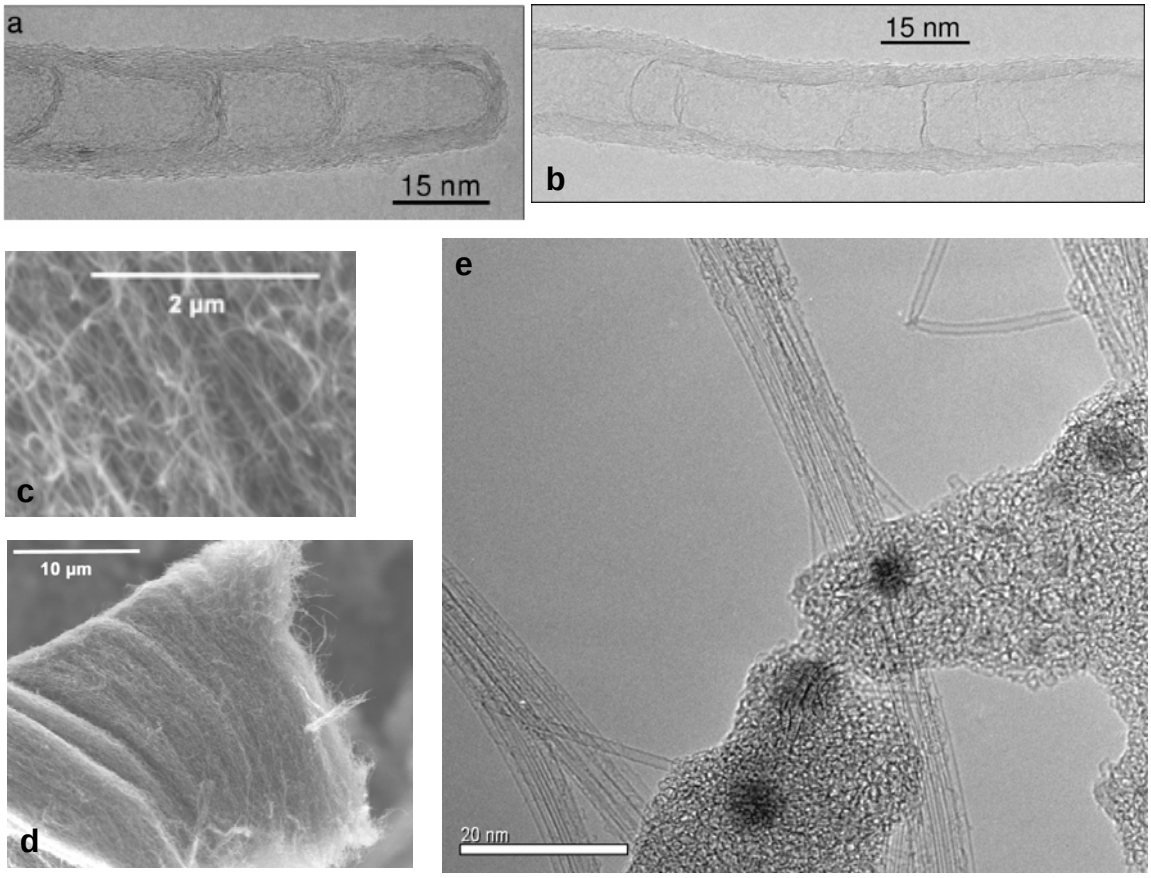

Figure 2. a), b) High resolution transmission microscopy images of nitrogen doped MWNTs (courtesy of M. Castignolles). c), d) Scanning electron microscopy images of aligned CNx nanotubes. Image c) is an enlargement of the tubes in d) the picture demonstrates that on a microscopic scale the tubes are not that well-aligned. All the multi-walled nanotubes shown here are synthesised using an aerosol technique utilizing acetonitril and tetrahydrofuran with different C/N ratios. e) HRTEM image of nitrogen doped SWNTs (courtesy of A. Khlobystov).

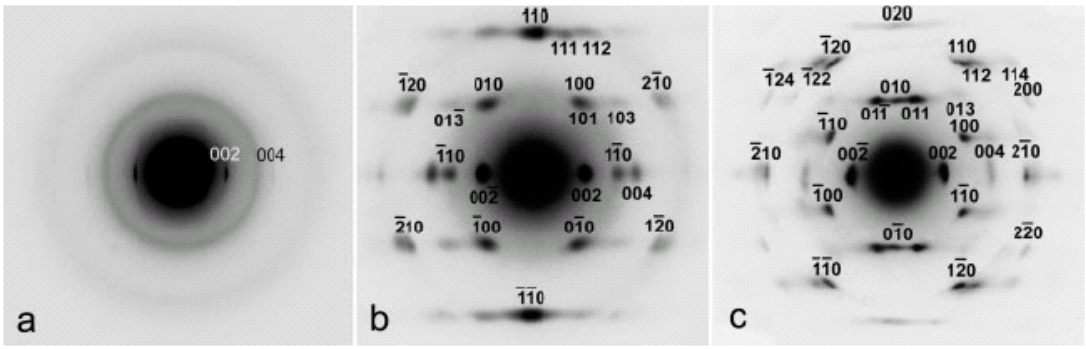

Figure 3. Electron diffraction pattern from individual multi-walled carbon nanotubes. (a) shows typical non-nitrogen doped tube showing no crystallographic register between the concentrically arranged tubes. (b) was typical of about 20% of tubes in their sample showing register between the MWNT layers of armchair orientation, (c) matched around 30% of their tubes showing zig-zag register. Reproduced with permission from Ref. [50],K. Koziol, *et al.*, *Advanced Mat.* 17(6) 760-763 (2005) ©2005 Wiley-VCH Verlag GmbH & Co. KGaA.

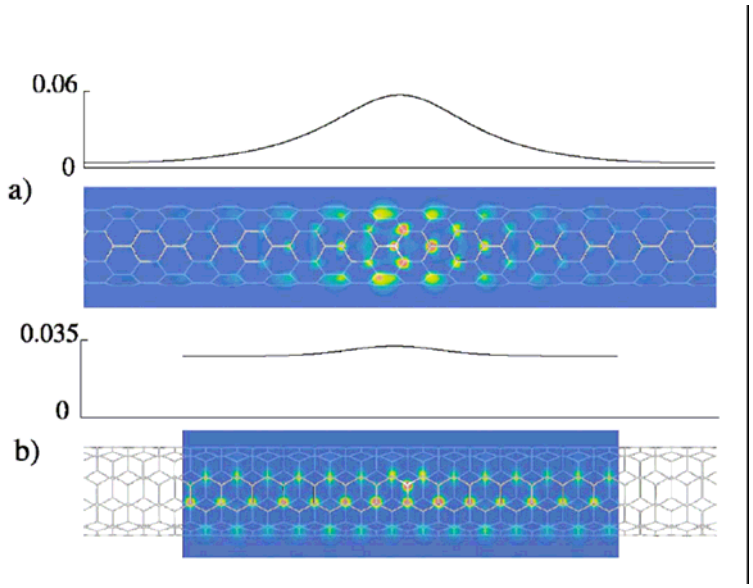

Figure 4. Diagram showing different spin density distribution of a substitutional nitrogen donor level in (a) semiconducting (8,0) zigzag nanotube and (b) metallic (5,5) armchair nanotube. **Reproduced with permission from Ref [67] A. H. Nevidomskyy, G. Csanyi, M. C. Payne, *Phys. Rev. Lett.* 91 105502 (2003) © 2003 The American Physical Society.**

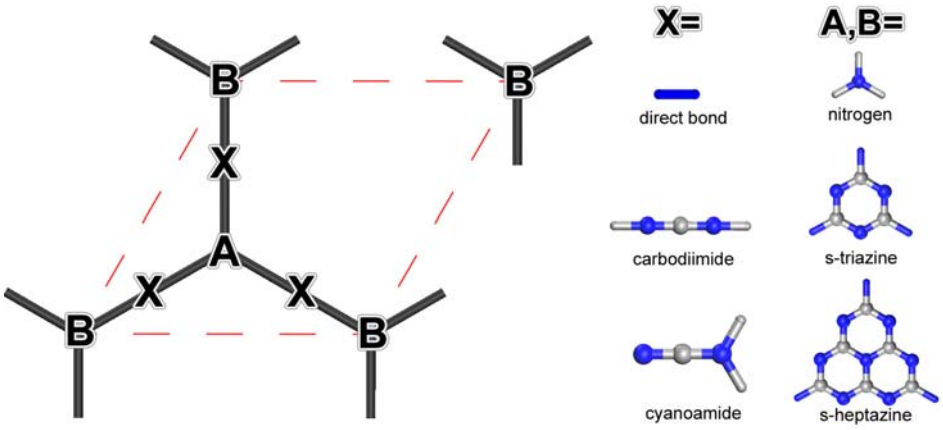

Figure 5 General schematic showing family of hexagonal layered CN_x compounds, substituting A and B with combinations of single nitrogen, s-triazine or s-heptazine, and interconnecting these either with a single bond, cyanoamide group or carbodiimide group.

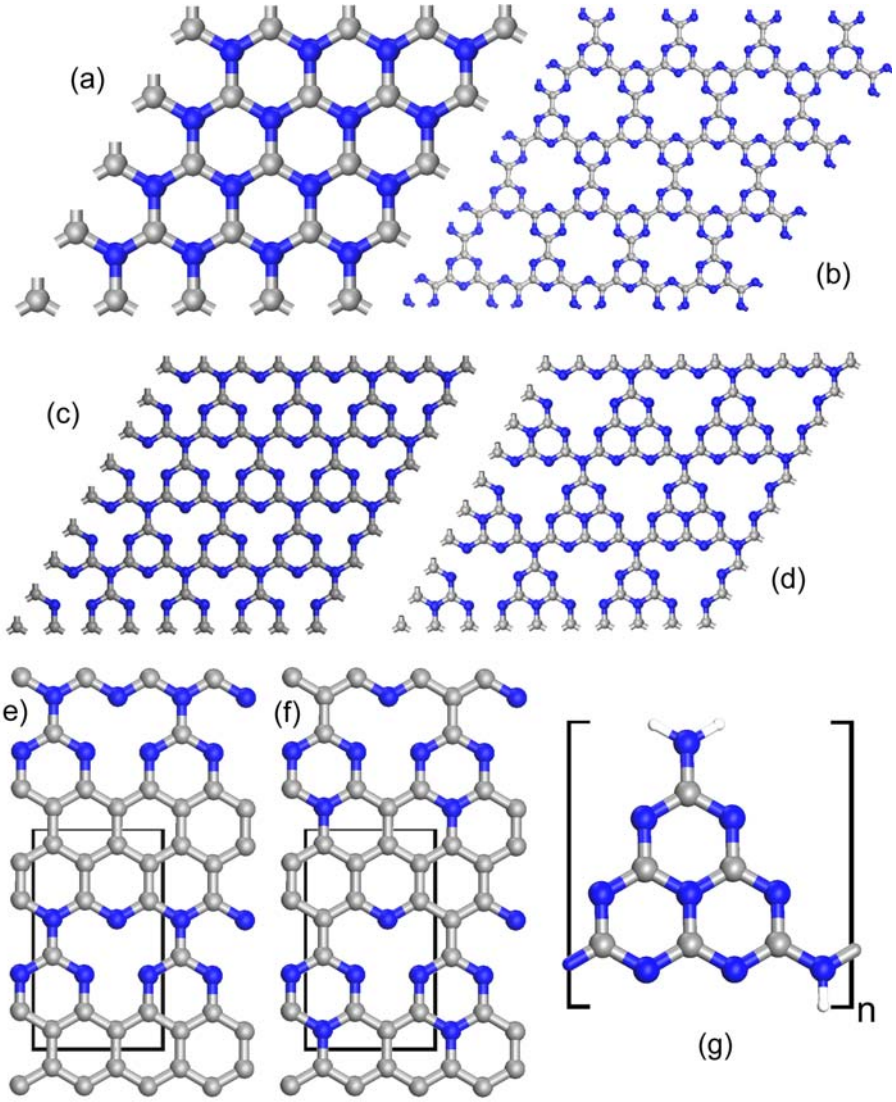

Figure 6 (a), (b) Two proposed monolayer CN structures. (a) is thermodynamically unstable with respect to, for example, crosslinking with neighbouring sheets, and will not remain planar. (c),(d) Proposed monolayer C_3N_4 structures. (c) features s-triazinunits, (d) containing s-heptazine units is thermodynamically more stable. (e), (f) Two proposed monolayer $C_{11}N_4$

lattices, isoelectronic with diamond, based around orthorhombic unit cells (shown in black) (g) Structural unit in melon, $C_6N_9H_3$ or poly[(8-amino-1,3,4,6,7,9,9b-heptaazaphenalen-2,5-diyl)imine].

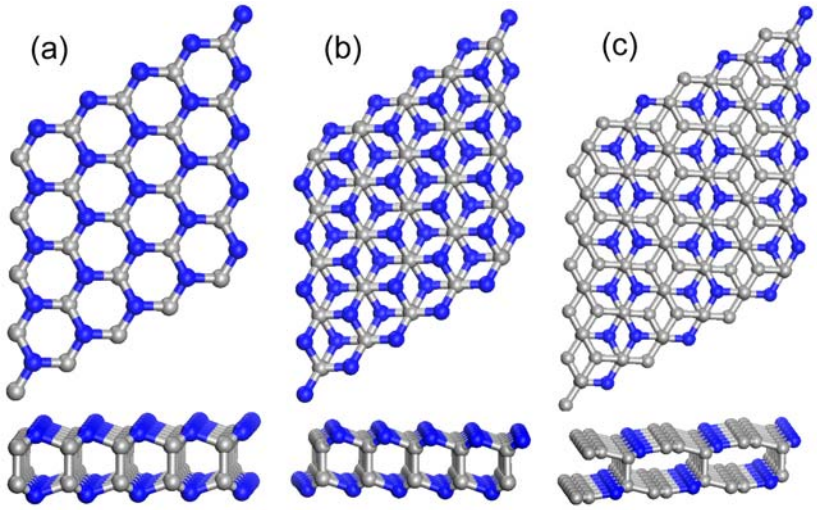

Figure 7 Bi-layer CN_x structures (top = top view, bottom = side view). (a) and (b) show CN based on α- and β-GeSe structure (i.e. alternate CN atoms with all carbon atoms cross-linked via C-C bonds, with layer offset equivalent to AA or AB stacking in graphite respectively), and (c) C_3N bilayer structure.

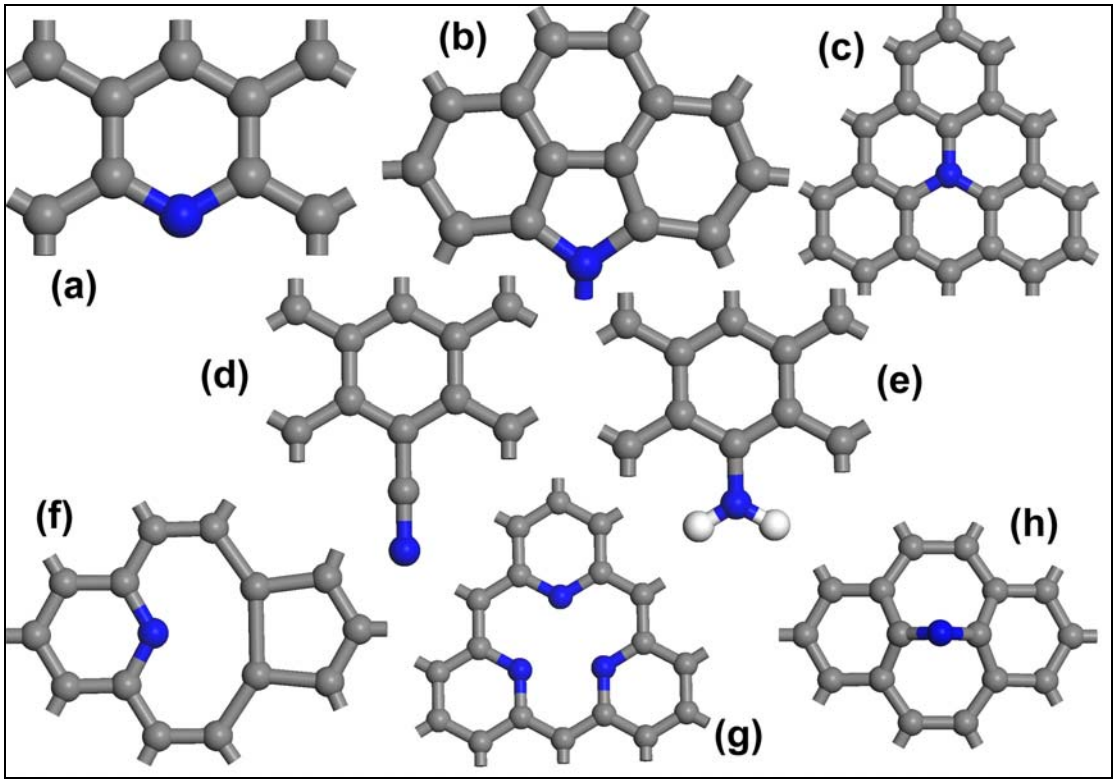

Figure 8 Possible bonding configurations for N in graphitic networks, (a) pyridinic-like N, (b) pyrrolic-type nitrogen (other pyrrolic configurations are possible provided the nitrogen remains

sp^3 coordinated), (c) graphitic substitutional nitrogen, (d) Nitrile -C≡N, (e) $–NH_2$, (f) pyridinic N-vacancy complex, (g) pyridinic N_3-vacancy, (h) interstitial nitrogen.

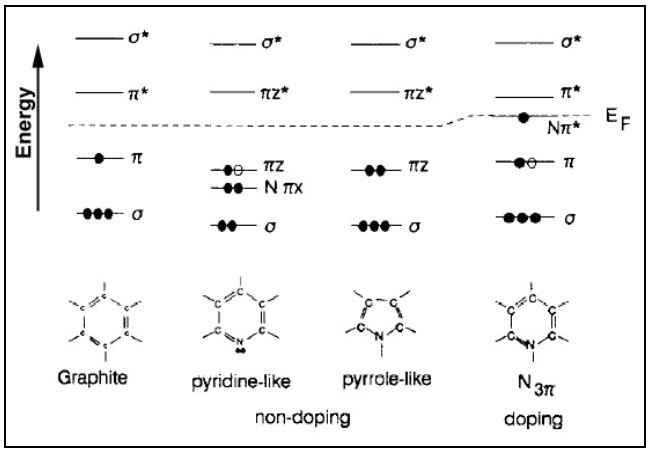

Figure 9 Molecular orbital diagrams showing electronic states associated with different bonding configurations of nitrogen in sp^2 carbon networks. Full and empty circles denote electrons from N and C respectively. Although only a qualitative guide (in reality these molecular states will interact strongly with the host material), it shows why only substitutional graphitic nitrogen leads directly to a donor state. However pyridinic-like nitrogen may still have associated acceptor states if next to a vacancy, due to the missing carbon p_z-orbital of the vacancy. Reproduced with permission from Ref [201], J. Robertson, C. A. Davis, *Diam. Rel. Mat.* 4 441 (1995) © 1995 Elsevier Science B.V.

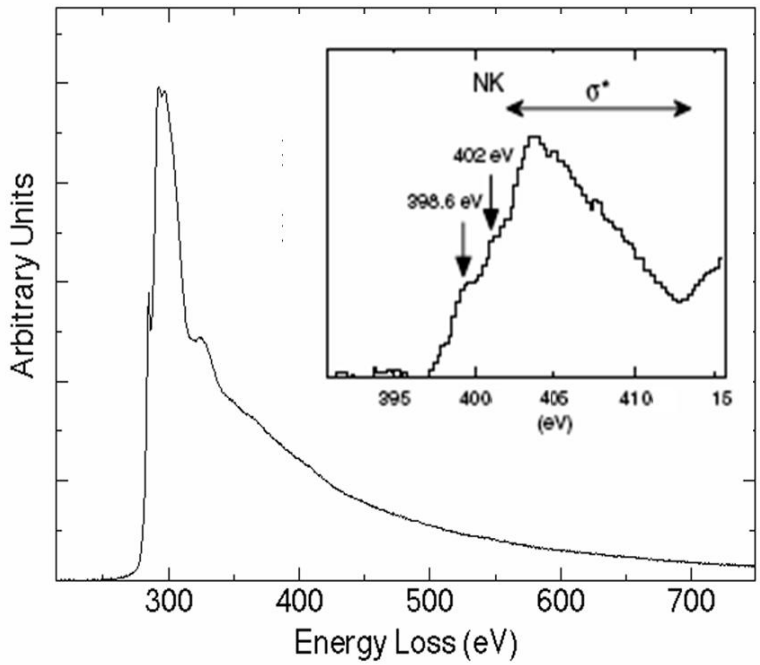

Figure 10. EEL core electron K-shell spectra of CN_x nanotube bundles. The nanotubes are doped with around 1 at.% nitrogen. For the C-K edge well defined p_ and r_ fine structure features are observed which are evidences of sp_2-hybridisation in graphitic structures. The inset is a magnification of the N-K edge. Reproduced with permission from [1], M. Glerup *et al. Chem. Phys. Lett.* 387, 193 (2004**) © 2004 Elsevier Science B.V..**

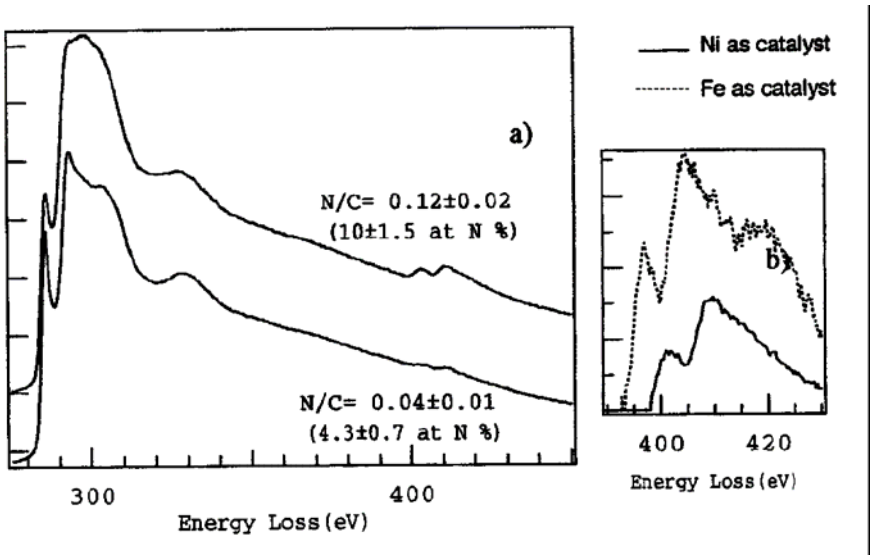

Figure 11. a) EEL spectra of nitrogen doped multi-walled nanotubes synthesised using nickel as the catalysts. b) N-K edge spectra of CNx tubes where the catalysts used were iron and nickel. Reproduced with permission after Ref.[55], Trasobares *et al. J. Chem. Phys.*, 116 (20), 8966 (2002) © *2006 American Institute of Physics*.

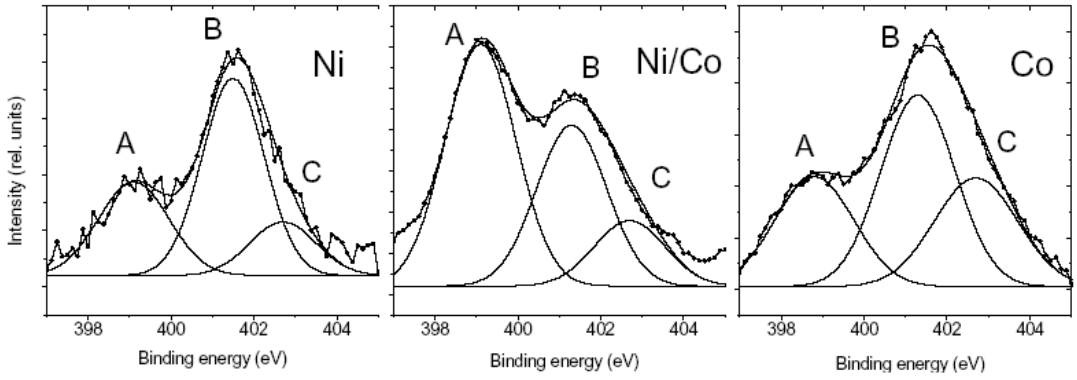

Figure 12 N1s spectra measured using X-ray photoelectron spectroscopy for N doped MWNT samples produced using Ni, Ni/Co and Co catalysts. The spectra were fitted by three Gaussian components at (A) 399.1 / 399.1 / 398.8, (B) 401.5 / 401.3 / 401.3 and (C) 402.7eV. Reproduced with permission from Ref [68], L. Bulusheva et al., Eur. Phys. J. D, 34 271-274 (2005) ©2005 European Physical Journal.

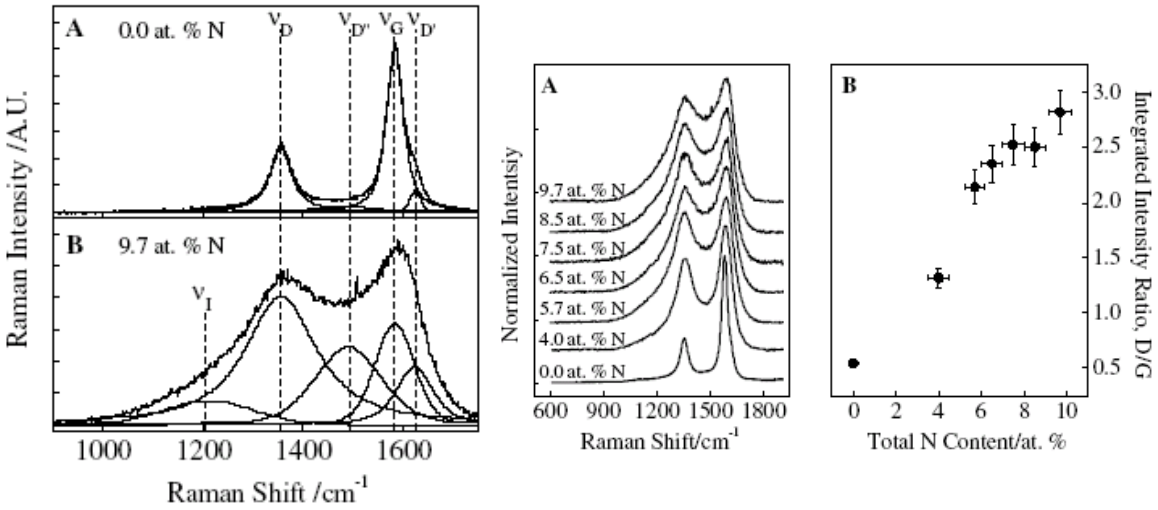

Figure 13. 1) Comparison of peak intensities and peak widths used in the fitting of the Raman spectra for MWNTs with A) 0 at% nitrogen and B) 9.7 at% nitrogen. 2) A) Normalised and baseline corrected Raman spectra with an increased nitrogen concentration. B) Ratio of the integrated intensities for the D and G bands versus nitrogen concentration. The nitrogen concentrations in the samples were determined using XP spectroscopy. Reproduced with permission from Ref. [115], S. Maldonado, S. Morin, K.J. Stevenson, *Carbon* 44 1429 (2006) © 2005 Elsevier Science BV.

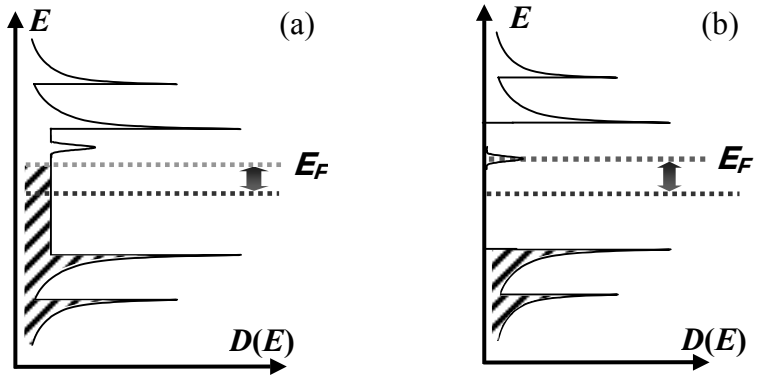

Figure 14. Schematic DOS *D*(*E*) as a function of energy *E* of a (a) metallic SWNT doped by substitution of carbon by nitrogen in a graphite-like way. The dotted lines represent the initial (dark grey) and the final (grey) position of the Fermi-energy E_F after ionization of the dopant states. The shift is indicated by an arrow. Hatched regions correspond to occupied states in the DOS. (b) Case of a semiconducting SWNT doped with nitrogen in a graphite-like way.

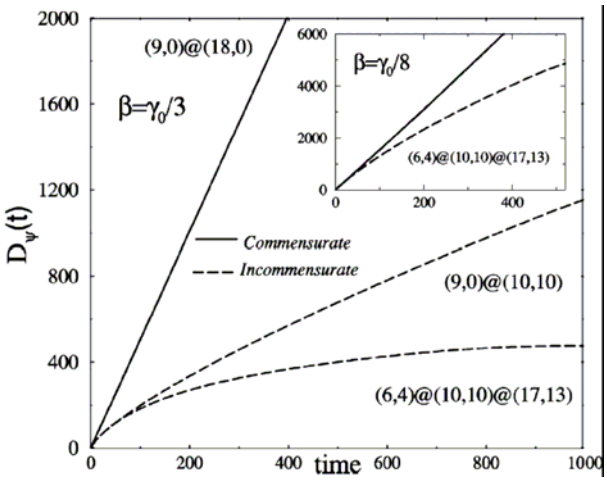

Figure 15 . Diffusion coefficients for double-walled and triple-walled commensurate and incommensurate CNTs as a function of time. Time is given in units $h/(2\pi\gamma_0)$, where h is the Planck's constant and γ_0 the tight-binding energy between two neighbouring carbon atoms in the honeycomb lattice. The parameter β is the measure for the imposed interaction strength between neighbouring shells. Inset: Diffusion coefficients for the (6,4)@(10,10)@(17,13) with weaker intershell interaction. Reproduced with permission from Ref [148], S. Roche *et al*., *Phys. Lett A* 285 94 (2001) © 2001 Elsevier Science B.V.

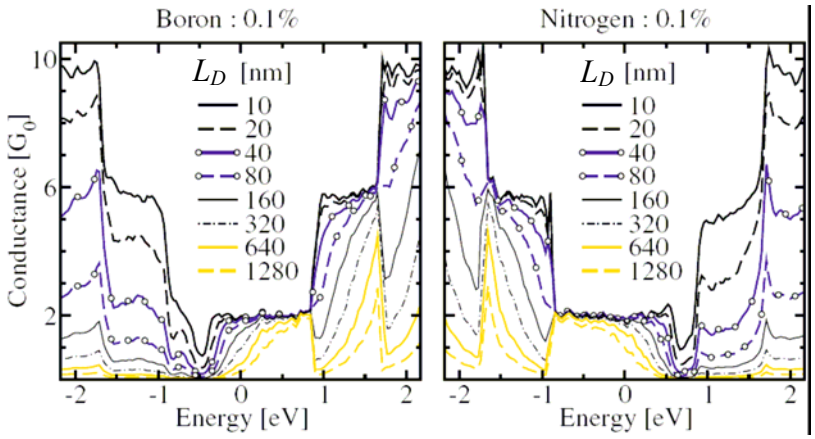

Figure 16. Left: quantum conductance of a (10,10) armchair SWNT with 0.1 atom% boron as function of the (normalised) Fermi-energy position. Right: quantum conductance of a (10,10) armchair SWNT with 0.1 atom% nitrogen as function of the (normalised) Fermi-energy position. Clearly at the energetic position where the nitrogen and boron states are a strong decrease in the conductance occurs due to increased scattering of the current carrying electrons. Reproduced with permission from Ref [163], S. Latil, D. Mayou, J. –C. Charlier, *Phys. Rev. Lett.* 92, 256805 (2004) © 2004 The American Physical Society.

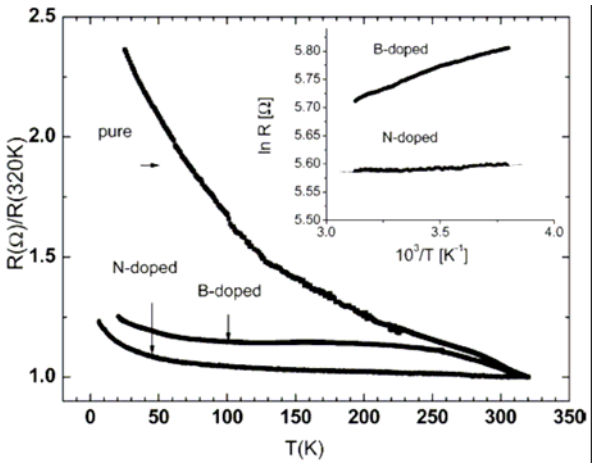

Figure 17. Temperature dependence of the resistance *R* for pristine, boron-doped and nitrogen-doped MWNTs mats (two-probe measurements). In all three cases a non-metallic behaviour is observed. Inset: logarithm of *R* vs reciprocal temperature, indicating that the dominant transport process in the mats may be a hopping process. Reproduced with permission from Ref [171], Y.M. Choi et al., *Nano Lett.* 3 839 (2003) © 2004 The American Chemical Society.

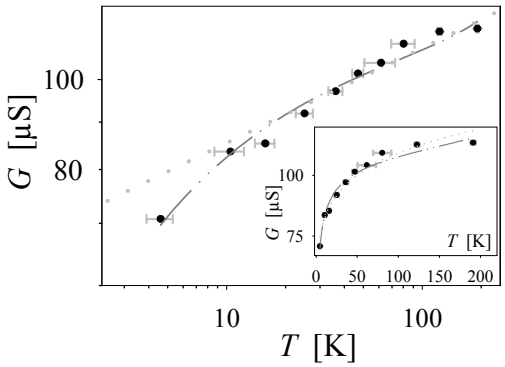

Figure 18. Temperature dependence of the zero-bias conductance of an individual, nitrogen-doped (metallic) SWNT. The dotted line corresponds to a power-law behaviour. The dash-dotted line to assumes a disordered wire system with electric-dipole interaction. Inset: Same data with linear axis [173].

1. M. Glerup, J. Steinmetz., D. Samaille, O. Stephan, S. Enouz, A. Loiseau, S. Roth, P. Bernier, *Chem. Phys. Lett.*, 387, 193 (**2004**)
2. M. Glerup , M.Castignolles, M. Holzinger,G. Hug,A. Loiseau,P. Bernier, *Chem. Comm.*, 20, 2542 (2003).
3. M. Castignolles, Thesis, Université Montpellier II, France, (**2004**).
4. R. Singh, D. Pantarotto, L. Lacerda, G. Pastorin, C. Klumpp, M. Prato, A. Bianco, K. Kostarelos, *PNAS*, 103, 3357 (**2006**).
5. F. H. J. Muller, N. Moreau, P. Misson, J.-F. Heilier, M. Delos, M. Arras, A. Fonseca, J. B. Nagy, D. Lison, *Toxicol. Appl. Pharmacol.*, 207, 221 (**2005**)

6. J. C. Carrero-Sanchez, R. Mancilla, G. Arrellin, H. Terrones, J. P. Laclette, M.Terrones, *Nano Lett.*, 6, 1609 (**2006**)
7. R. S. Lee, H. J. Kim, J. E. Fischer, J. Lefebvre, M. Radosavljevic, J. Hone, A. T. Johnson, *Phys. Rev. B*, 61, 4526 (**2000**)
8. M. Bockrath, J. Hone, A. Zettl, P. L. McEuen, A. G. Rinwler, R. E. Smalley, *Phys. Rev. B*, 61, R10606 (**2000**).
9. S. Ciraci, S. Dag, T. Yildirim, O. Gülseren, R. T. Senger, *J. Phys. Cond. Matt*, 16, R901 (**2004**).
10. T. Lin, V. Bajpai, T. Ji, L. Dai, *Aust. J. Chem.*, 56, 635 (2003)
11. J. I. Paredes, F. S. Garcia, S. V-Rodil, A. Matrinez-Alonso, J. Tascon, E. J. Bottani, *J. Phys. Chem. B*, 107, 8905 (**2003**).
12. O. Stephan, P. M. Ajayan, C. Colliex, P. Redlich, J. M. Lambert, P. Bernier, P. Lefin, *Science,* 266, 1683 (**1994**).
13. R. Droppa Jr., P. Hammer, A.C.M. Carvalho, M.C. dos Santos, F. Alvarez, *J. Non-Crystalline Solids*, 299, 874 (**2002**).
14. C. J. Lee, S. C. Lyu, H.-W Kim, J. H. Lee, K. I. Cho, *Chem. Phys. Lett.*, 359, 115 (**2002**).
15. K. Jiang, L. S. Schadler, R. W. Siegel, X. Zhang, H. Zhang, M. Terrones, *J. Mater. Chem.* , 14, 37 (**2004**).
16. M. Holzinger, J. Steinmetz, S. Roth, M. Glerup, R. Graupner, *AIP Conf. Proc.*, 786, 211 (**2005**).
17. R. Czerw, M. Terrones, J. –C. Charlier, X. Blase, B. Foley, R. Kamalakaran, N. Grobert, H. Terrones, D. Tekleab, P. M. Ajayan, W. Blau, M. Ruhle, D. L. Carroll, *Nano Lett.*, 1, 457 (**2001**).
18. M. Terrones, P. M. Ajayan, F. Banhart, X. Blase, D. L. Carroll, J. –C. Charlier, R. Czerw, B. Foley, N. Grobert, R. Kamalakaran, P. Kohler-Redlich, M. Rühle, T. Seeger, H. Terrones, *Appl. Phys. A*, 74, 355 (**2002**).
19. D. Srivastava, M. Menon, C. Dariao, S. Jin, B. Sadanadan, A. M. Rao, *Phys. Rev. B*, 69, 153414 (**2004**).
20. C. Journet, W. K. Maser, P. Bernier, A. Loiseau, M. Lamy de la Chapelle, S. Lefrant, P. Deniard, R. Lee, J. E. Fischer, *Nature*, 388, 756 (**1997**).
21. J. Bill, R. Riedel, *Mater Res Soc Symp Proc,* 271, 839 (**1992**).
22. K. Suenaga, C. Colliex, N. Demoncy, A. Loiseau, H. Pascard, F. Willaime, *Science*, 278, 653 (**1997**).
23. Y. Zhang, H. Gu, K. Suenaga, S. Iijima., *Chem. Phys. Lett.*, 279, 264 (**1997**).
24. S. Glenis, S. Cooke, X. Chen, M. M. Labes, *Chem. Mater.*, 6, 1850 (**1994**).
25. T. Pradeep, V. Vijayakrishnan, A. K. Santa, C. N. R. Rao, *J. Phys. Chem.*, 95 (**1991**).
26. R. Yu, M. Zhan, D. Cheng, S. Yang, Z. Liu, L. Zheng, *J. Phys. Chem.*, 99, 1818 (**1995**).
27. Z. C. Ying, R. L. Hettich, R. N. Compton, R. E. Haufler, *J. Phys. B. At. Mol. Opt. Phys.*, 29, 4935 (**1996**).
28. J. C. Hummelen, B. Knight, J. Pavlovich, R. Gonzalez, F. Wudl, *Science*, 269, 1554 (**1995**).
29. M. Terrones, H. Terrones, N. Grobert, W. K. Hsu, Y. Q. Zhu, J. P. Hare, H. W. Kroto, D. R. M. Walton, Ph. Kohler-Redlich, M. Rühle, J. P.Zhang, A. K. Cheetham, *Appl. Phys. Lett.*, 75, 3932 (**1999**).
30. M. Yudasaka, R. Kikuchi, Y. Ohki, S. Yoshimura, *Carbon*, 35, 195 (**1997**).
31. C. Tang, Y. Bando, D. Golberg, F. Xu, *Carbon*, 42, 2625 (**2004**).

32. S.Y. Kim, J. Lee, C.W. Na, J. Park, K. Seo, B. Kim, *Chem. Phys. Lett.,* 413, 300 (**2005**).
33. A. G. Kudashov, A. V. Okotrub, L. G. Bulusheva, I. P. Asanov, Yu. V. Shubin, N. F. Yudanov, L. I. Yudanova, V. S. Danilovich, O. G. Abrosimov, *J. Phys. Chem. B*, 108, 9048 (**2004**).
34. Y. Jiang, Y. Wu, S. Zhang, C. Xu, W. Yu, Y. Xie, Y. Qian, *J. Am. Ceram. Soc.*, 122, 12383 (**2000**).
35. X. Wang, J. Lu, Y. Xie, G. Du, Q. Guo, S. Zhang, *J. Phys. Chem. B,* 106, 2186 (**2002**).
36. C. Cao, F. Huang, C. Cao, J. Li, H. Zhu, *Chem. Mater.*, 16, 5213 (**2004**).
37. Q. Guo, Y. Xie, X. Wang, S. Zhang, T. Hou, Lv. Shichang, *Chem. Comm.*, 1, 26 (**2004**).
38. T. Mu, J.Huang, Z. Liu, Z. Li, B. Han, *J. Mater. Res.*, 21, 1658 (**2006**).
39. D. Goldberg, Y. Bando, L. Bourgeois, K. Kurashima, T. Sato, *Carbon*, 38, 2017 (**2000**).
40. K. Suenaga, M. P. Johansson, N. Hellgren, E. Broitman, L. R. Wallenberg, C. Colliex, J. –E. Sundgren, L. Hultman, *Chem. Phys. Lett.*, 300, 695 (**1999**).
41. L. Hultman, S. Stafstrom, Z. Czigany, J. Neidhardt, N. Hellgren, I. F. Brunell, K. Suenaga, C. Colliex, *Phys. Rev. Lett.*, 87, 225503 (**2001**).
42. J. Kotakoski, J. A. V. Pomoell, A. V. Krasheninnikov, K. Nordlund, *Nucl. Instr. and Meth. B*, 228, 31(**2005**)
43. J. Kotakoski, A. V. Krasheninnikov, Y. Ma, A. S. Foster, K. Nordlund, R. M. Nieminen*, Phys. Rev. B*, 71, 205408 (**2005**).
44. C. Morant, J. Andrey, P. Prieto, D. Mendiola, J. M. Sanz, E. Elizalde, *Physica Status Solidi A*, 203, 1069 (**2006**).
45. K. Yamamoto, T. Kamimura, K. Matsumoto, *Jap. J. Appl. Phys*, 4A, 1611 (**2005**).
46. H. C. Choi, S. Y. Bae, J. Park, K. Seo, C. Kim, B. Kim, H.J. Song, H.-J. Shin, *Appl. Phys. Lett.*, 85, 5742 (**2004**).
47. H. C. Choi, J. Park, B. Kim, *J. Phys. Chem. B*, 109, 4333 (**2005**).
48. R. Sen, B. C. Satishkumar., A. Govindaraj, K. R. Harikumar, G. Raina, J.-P Zhang, A. K. Cheetham, C. N. R. Rao, *Chem. Phys. Lett.*, 287, 671 (**1998**).
49. X. Ma, E. Wang, W. Zhou, D. Jefferson, J. Chen, S. Deng, N. Xu, J. Yuan, *Appl. Phys. Lett.*, 75, 3105 (**1999**).
50. K. Koziol, M. Shaffer, A. Windle, *Adv. Mater.*, 17, 760 (**2005**).
51. C. Ducati, K. Koziol., S. Friedrichs, T.J.V. Yates, M.S. Shaffer, P.A. Midgley A.H. Windle, *Small,* 2, 774 (**2006**).
52. Y. Saito, *Carbon*, 33, 979 (**1995**).
53. M. Terrones, A. M. Benito, C. Manteca-Diego, W. K. Hsu, O. I Osman, J. P. Hare, D. G. Reid, H. Terrones, A. K. Cheetham, K. Prassides, H. W. Kroto, D. R. M. Walton, *Chem. Phys. Lett.*, 257, 576 (**1996**).
54. D. Zhong, S. Liu, G. Zhang, E. G. Wang, *J. Appl. Phys.*, 89, 5939 (**2001**).
55. S. Trasobares, O. Stephan, C. Colliex, W. K. Hsu, H. W. Kroto, D. R. M. Walton, *J. Chem. Phys.*, 116, 8966 (**2002**).
56. A. G. Kudashov, O. G. Abrosimov, R. G. Gorbachev, A. V. Okotrub, L. I. Yudanova, A. L. Chuvilin, A. I. Romanenko, *Full. Nanotubes and carbon nanostructures*, 12, 93 (**2004**).
57. N. Grobert, M. Terrones, S. Trasobares, K. Kordatos, H. Terrones, J. Olivares, J. P. Zhang, P. Redlich, W. K. Hsu, C. L. Reeves, D. J. Wallis, Y. Q. Zhu, J. P.

Hare, A. J. Pidduck, H. W. Kroto, D. R. M. Walton, *Appl. Phys. A*, 70, 175 (**2000**).
58. G. Düsberg, *private communication* (**2005**).
59. S. Amelickx, X. B. Zhang, D. Bernaerts, X. F. Zhang, V. Ivanov, J. B. Nagy, *Science*, 265, 635 (**1994**).
60. R. Kurt, C. Klinke, J.-M. Bonard, K. Kern, A. Karimi, *Carbon*, 39, 2163 (**2001**).
61. P. L. McEuen, M. Bockrath, D. H. Cobden, Y. –G. Yoon, S. G. Louie, *Phys. Rev. Lett.*, 83, 5098 (**1999**).
62. X. Blase, J. -C. Charlier, A. De Vita, R. Car, P. Redlich, M. Terrones, W. K. Hsu, H. Terrones, D. L. Carroll, P. M. Ajayan, *Phys. Rev. Lett.*, 83, 5078 (**1999**).
63. D. Goldberg, P. S. Dorozhkin, Y. Bando, Z. –C. Dong, C. C. Tang, Y. Uemura, N. Grobert, M. Reyes-Reyes, H. Terrones, M. Terrones, *Appl. Phys. A*, 76, 499 (**2003**).
64. K. Koziol, M. Shaffer, A. Windle, *Adv. Mater.*, 17, 760 (**2005**).
65. J. G. Wiltshire, L. Li, L. Herz, R. Nicholas, M. Glerup, J. Sauvajol, A. Khlobystov, *Phys. Rev. B*, 72, 205431 (**2005**).
66. L. -J. Li, M. Glerup, A.N. Khlobystov, J.G. Wiltshire, J.-L. Sauvajol, R.A. Taylor, R.J. Nicholas, *Carbon*, 44, 2752 (**2006**).
67. A. H. Nevidomskyy, G. Csányi, M.C. Payne, *Phys. Rev. Lett.*, 91, 105502 (**2003**).
68. L. G. Bulusheva, A.V.Okotrub, A. G. Kudashov, I. P. Asanov, O. G. Abrosimov, *Eur. Phys. Journal D*, 34, 271 (**2005**).
69. P. E. Lammert, V. H. Crespi, A. Rubio, *Phys. Rev. Lett.*, 87, 136402 (**2001**).
70. M. L. Cohen, *Phys. Rev. B*, 32? 7988 (**1985**).
71. D. M. Teter, *MRS Bull. Jpn.*, 98, 22 (**1998**).
72. E. Kroke, M. Schwarz, *Coord. Chem. Rev.*, 248, 493 (**2004**).
73. S.D. Mo, L. Ouyang, W.Y.Ching, I. Tanaka, Y. Koyama, R. Riedel, *Phys. Rev. Lett.*, 83, 5046 (**1999**).
74. J. J. Kroll, *Solid State Chem.*, 176, 530 (**2003**).
75. D.M. Teter, R. J. Hemley, *Science*, 271, 53 (**1996**).
76. A.Y. Liu, R. M. Wentzcovitch, *Phys. Rev. B*, 50, 10362 (**1994**).
77. J. Ortega, O. F. Sankey, *Phys. Rev. B*, 51, 2626 (**1995**).
78. J. E. Lowther, *Phys. Rev. B*, 59, 11683 (**1999**).
79. E. Kroke, M. Schwarz, P. Kroll, E. Bordon, B. Bordon, B. Noll, A. Norman, *New J. Chem.*, 26, 508 (**2002**).
80. I. Alves, G. Demazeau, B. Tanguy, F. Weill, *Solid State Commun.*, 109, 697 (**1999**).
81. M. Mattesini, S. F. Matar, J. Etourneau, *J. Mater. Chem.*, 10, 709 (**2000**).
82. R. Riedel, E. Kroke, A. Greiner, A.O. Gabriel, L. Ruwisch, J. Nicolich, P. Kroll, *Chem Mater*., 10, 2964 (**1998**).
83. E. Kim, C. Chen, Töhler, M. Elstner, T. Frauenheim, *Phys. Rev. Lett.,* 86, 652 (**2001**).
84. R. Weihrich, V. Eyert, S.F. Matar, *Chem. Phys. Lett.*, 373, 636 (**2003**).
85. M. C. dos Santos, F. Albarez, *Phys. Rev. B*, 58, 13918 (**1998**).
86. Y. Miyamoto, M. L. Cohen, S. G. Louie, *Solid State Commun.*, 102, 605 (**1997**).
87. M. Côté, M. L. Cohen, *Phys. Rev. B*, 55, 5684 (**1997**).

88. Z. J. Zhang, P. Yang., C. M. Lieber, *Mater. Res. Soc. Symp. Proc.*, 388, 271 (**1995**).
89. W. B. Pearsson, *Acta Cryst.*, 17, 1 (**1964**).
90. E. Sandre, C. J. Pickard, C. Colliex, *Chem. Phys. Lett.*, 325, 53 (**2000**).
91. E. Hernández, C. Goze, P. Bernier, A. Rubio, *Phys. Rev. Lett.*, 80, 4502 (**1998**).
92. E. Hernández, C. Goze, P. Bernier, A. Rubio, *App. Phys. A*, 68, 287 (**1999**).
93. J. P. Lu, *Phys. Rev. Lett.*, 79, 1297 (**1997**).
94. Y. Guo, W.A.G.I., *Chem. Phys. Lett.*, 237, 72 (**1995**).
95. M. Zhao, Y. Xao, J. P. Lewis, R. Zhang, *J. Appl. Phys.*, 94, 2398 (**2003**).
96. S. Trasobares, Thesis, Université Paris Sud, France, (**2001**).
97. M. W. Zhao, Y. Y. Xao, Y. C. Ma, M. J. Ying, X. D. Liu, L. M. Mei, *Phys. Rev. B*, 66, 155403 (**2002**).
98. H. S. Kang, S. Jeong, *Phys. Rev. B*, 70, 233411 (**2004**).
99. J. -Y. Yi, J. Bernholc, *Phys. Rev. B*, 47, 1708 (**1993**).
100. A. H. Nevidomskyy, G. Czani., M. C. Payne, *Phys. Rev. Lett.*, 91, 105502 (**2003**).
101. J.-Y. Yi, J. Bernholc., *Phys. Rev. B*, 47, 1708 (**1993**).
102. C. P. Ewels, unpublished, (**2005**).
103. W. J. Gammon, O. Kraft, A. C. Reilly, B. C. Holloway, *Carbon*, 41, 1917 (**2003**)..
104. A. A. El-Barbary, R. H. Telling, C. P. Ewels, M. I. Heggie, P. R. Briddon, *Phys. Rev. B*, 68, 144107 (**2003**).
105. A. T. Balaban, *Match*, 33, 25 (**1996**).
106. M. Terrones, A. Jorio, M. Endo, A.M. Rao, Y. A. Kim, T. Hayashi, H. Terrones, J. –C. Charlier, G. Dresselhaus, M. S. Dresselhaus, *Materials Today*, 30 (**2004**).
107. Y. Miyamoto, S. Berber, M. Yoon, A. Rubio, D. Tomanek, *Physica B : Cond. Mat.*, 323, 78 (**2002**).
108. M. Castignolles, S.Enouz., O. Stéphan, C. P. Ewels, A. Loiseau, C. Colliex, *unpublished*, (**2005**).
109. R. Droppa Jr, C. T. M. Ribeiro, A. R. Zanatta, M. C. dos Santos, F. Alvarez, *Phys. Rev. B*, 69, 045405 (**2004**).
110. M. Terrones, P. Redlich, N. Grobert, S. Trasobares, W. –K. Hsu, H. Terrones, Y. –Q. Zhu, J. P. Hare, C. L. Reeves, A. K. Cheetham, M. Rühle, H. W. Kroto, D. R. M. Walton, *Adv. Mat.*, 11, 655 (**1999**).
111. X. Wang, Y.Liu, D. Zhu, L. Zhang, H. Ma, N. Yao, B. Zhang, *J. Phys. Chem. B*, 106, 2186 (**2002**).
112. J. Casanovas, J. M. Ricart, J. Rubio, F. Illas, J. M. Jimenez-Mateos, *J. Am. Chem. Soc.*, 118, 8071 (**1996**).
113. I. Jiménez, W. M. Tong, D. K. Shuh, B. C. Holloway, M. A. Kelly, P. Pianetta, L. J. Terminello, F. J. Himpsel, *Appl. Phys. Lett.*, 74, 2620 (**1999**).
114. S.H. Lim, H. I. Elim, X.Y. Gao, A.T.S. Wee, W. Ji, J.Y. Lee J. Lin, *Phys. Rev. B*, 73, 045402 (**2006**).
115. S. Maldonado, S. Morin, K. J. Stevenson, *Carbon*, 44, 1429 (**2006**).
116. X. Wu, Y.Tao, Y. Lu, L. Dong, Z. Hu, *Diamond Relat. Mater.*, 15, 164 (**2006**).
117. J. Liu, S. Webster, D.L. Carroll, *J. Phys. Chem. B*, 109, 15769 (**2005**).
118. J. Liu, S. Webster, D.L. Carroll, *Appl. Phys. Chem.*, 88, 213119 (**2006**).

119. Q.-H. Yang, P. -X. Hou, M. Unno, S. Yamauchi, R. Saito, T. Kyotani, *Nano Lett.*, 5, 2465 (**2005**).
120. A. Misra, P. K. Tyagi, M. K. Singh, D. S. Misra, *Diamond Relat. Mater.*, 15, 385 (**2006**).
121. X. Wu, Y.Tao, Y. Lu, L. Dong, Z. Hu, *Diamond Relat. Mater.*, 15, 164 (**2006**).
122. L. H. Chan, K. H. Hong, D. Q. Xiao, T. C. Lin, S. H. Lai, W. J. Hsieh, H. C. Shih, *Phys. Rev. B*, 70, 125408 (**2004**).
123. A. Snis, S. F. Matar, O. Plashkevych, H. Ågren, *J. Chem. Phys.*, 111, 9678 (**1999**).
124. F. Le Normand, J. Hommet, T. Szörényi, C. Fuchs, E. Fogarassy, *Phys. Rev. B*, 64, 235416 (**2001**).
125. P. Bagus, *Phys. Rev. B*, 139, A619 (**1965**).
126. A. Johansson, S. Stafström, *J. Chem. Phys.*, 111, 3203 (**1999**).
127. N. Hellgren, J. Guo, C. Sathe, A. Agui, J. Nordgren, Y. Luo, H. Agren, J.-E. Sundgren, *Appl. Phys. Lett.*, 79, 4348 (**2001**).
128. Y. Miyamoto, A. Rubio, S. G. Louie, M. L. Cohen., *Phys. Rev. B*, 60, 13885 (**1999**).
129. N. Hellgren, M. P. Johannsson, E. Broitman, L. Hultman, J. –E. Sundgren, *Phys. Rev. B*, 59, 5162 (**1999**).
130. C. P. Ewels, O. Stephan, C. Colliex, *in preparation*, (**2006**).
131. D. L. Carroll, D.L., *Mol. Nanostruct., Proc. Int. Wintersch. Electron. Prop. Novel Mater.*, 477 (**1998**).
132. E. T. Mickelson, I. W. Chiang, J. L. Zimmerman, P. H. Boul, J. Lozano, J. Liu, R. E. Smalley, R. H. Hauge, J. L. Margrave, *J. Phys. Chem. B*, 103, 4318 (**1999**).
133. A. V. Okotrub, N. Maksimova, T. A. Duda, A. G. Kudashov, Yu. V. Shubin, D. S. Su, E. M. Pazhetnov, A. I. Boronin, L. G. Bulusheva, *Fullerenes, Nanotubes and Carbon Nanostructures*, 12, 99 (**2004**).
134. K. Jiang, A. Eitan, L. S. Schadler, P. M. Ajayan, R. W. Siegel, N. Grobert, M. Mayne, M. Reyes-Reyes, H. Terrones, M. Terrones, *Nano Lett.*, 3, 275 (**2003**).
135. F. Villalpando-Páez, A. H. Romero, E. Muñoz-Sandoval, L. M. Martínez, H. Terrones, M. Terrones, *Chem. Phys. Lett.*, 386, 137 (**2004**).
136. R. Saito, G.Dresselhaus, M.S. Dresselhaus, *"Physical Properties of Carbon Nanotubes", Imperial College Press (London)*, 17 (**1998**).
137. A. Bachtold, M. S. Fuhrer, S. Plyasunov, M. Forero, E.H. Anderson, A. Zettl, *Phys. Rev. Lett.*, 84, 6082 (**2000**).
138. V. Krstić, S. Roche, M. Burghard, *Phys. Rev. B*, 62, R16353 (**2000**).
139. M. S. Fuhrer, M. Forero, A. Zettl, P.L. McEuen, *Electronic Properties of Molecular Materials*, ed. by H. Kuzmany, J. Fink, M. Mehring, S. Roth, AIP, 591, 401 (**2001**).
140. R. Egger, A. Bachtold, M.S. Fuhrer, M. Bockrath, D.H. Cobden, P.L. McEuen, *Interacting electrons in Nanostructures*. Lecture Notes in Physics, Springer-Verlag, 579 (**2001**).
141. R. Saito, G. Dresselhaus, M.S. Dresselhaus, *Physical Properties of carbon Nanotubes*. 2 ed., London: Imperial College Press (**1998**).
142. T. Hertel, G. Moos, *Phys. Rev. Lett.*, 84, 5002 (**2000**).
143. C. L. Kane, M. P. A. Fisher, *Phys. Rev. B*, 68, 15233 (**1992**).
144. C. L. Kane, M. P. A. Fisher, *Phys. Rev. Lett.*, 68, 1220 (**1992**).
145. F. D. M. Haldane, *Phys. Rev. Lett.*, 47, 1840 (**1981**).

146. S. Sanvito, Y. K. Kwon, D. Tomanek, C.J. Lambert, *Phys. Rev. Lett.*, 84, 1974 (**2000**).
147. V. H. Crespi, M. L. Cohen, A. Rubio, *Phys. Rev. Lett.*, 79, 2093 (**1997**).
148. S. Roche, F. Triozon, A. Rubio, D. Mayou, *Phys. Lett. A*, 285, 94 (**2001**).
149. S. Frank, P. Poncharal, Z.L. Wang, W.A. de Heer, *Science*, 280, 1744 (**1998**).
150. A. Bachtold, C. Strunk, J.-P. Salvetat, J.-M. Bonard, L. Forró, T. Nussbaumer, C. Schönenberger, *Nature*, 397, 673 (**1999**).
151. C. Schönenberger, A. Bachtold, C. Strunk, J.P. Salvetat, L. Forró, *Appl. Phys. A*, 69, 283 (**1999**).
152. A. Bachtold, M. de Jonge, K. Grove-Rasmussen, P. L. McEuen, M. Buitelaar, C. Schönenberger, *Phys. Rev. Lett.*, 87, 166801 (**2001**).
153. S. Sanvito, Y-K Kwon, D. Tománek, C. J. Lambert, *Phys. Rev. Lett.*, 84, 1974 (**2000**).
154. E. G. Mishchenko, A. V. Andreev, L. I. Glazman, *Phys. Rev. Lett.*, 87, 246801 (**2001**).
155. V. Krstić, S. Blumentritt, J. Muster, S. Roth, A. Rubio, *Phys. Rev. B*, 67, 041401(R) (**2000**).
156. M. F. Lin, D. S. Chuu, *Phys. Rev. B*, 56, 4996 (**1997**).
157. M. Büttiker, *Phys. Rev. Lett.*, 57, 1761 (**1986**).
158. M. Büttiker, *IBM J. Res. Develop*., 32, 317 (**1988**).
159. G. Grüner, *Frontiers in Physics*, in *Density Waves in Solids,*. Addison-Wesley Publishing Company (Massachusetts, Menlo Park, New York) (**1994**).
160. M. Bockrath, D. H. Cobden, A. G. Rinzler, R. E. Smalley, L. Balents, P. L. McEuen, *Nature*, 397, 598 (**1999**).
161. C. Kaun, B. Larade., H. Mehrez, J. Taylor, H. Guo, *Phys. Rev. B*, 65, 205416 (**2002**).
162. H. J. Choi, J. Ihm, S. G. Louie, M. L. Cohen, *Phys. Rev. Lett.*, 84, 2917 (**2000**).
163. S. Latil, S.Roche, D. Mayou, J. -C. Charlier, *Phys. Rev. Lett.*, 92, 256805 (**2004**).
164. A. A. Farajian, K. Eesfarjani, Y. Kawazoe, *Phys. Rev. Lett.*, 82, 5084 (**1999**).
165. Y. Liu, H.Guo, *Phys. Rev. B*, 69, 115401 (**2004**).
166. Y. Miyamoto, *Phys. Rev. B*, 54, R11149 (**1996**).
167. V. Krstić, S. Roche, M. Burghard, K. Kern, G.L.J.A. Rikken, *J. Chem. Phys.*, 117, 11315 (**2002**).
168. C. P. Ewels, M. Glerup. *Journal of Nanoscience and Nanotechnology*, 5, 1345 (**2005**).
169. K. McGuire, N. Gothard, P.L. Gai, M.S. Dresselhaus, G. Sumanasekera, A.M. Rao, *Carbon*, 43, 219 (**2005**).
170. S.Y. Kim, J. Lee, C.W. Na, J. Park, K. Seo, B. Kim, *Chem. Phys. Lett.*, 413, 300 (**2005**).
171. Y.M. Choi, D. -S. Lee, R. Czerw, P.W. Chiu, N. Grobert, M. Terrones, M. Reyes-Reyes, H. Terrones, J.-C. Charlier, P. M. Ajayan, S. Roth, D.L. Carroll, Y.W. Park, *Nano Lett.*, 3, 839 (**2003**).
172. K. Xiao, Y.Liu, P. Hu, G.Yu, Y. Sun, D. Zhu, *J. Am Chem. Soc.*, 127, 8614 (**2005**).
173. V. Krstić, G.L.J.A. Rikken, P. Bernier, S. Roth, M. Glerup, *cond-mat/0601513. to be published* (**2006**).
174. R. H. Xie, *Chem. Phys. Lett.*, 310, 379 (**1999**).
175. G. Zhou, W. Duan, *J. Nanosci. Nanotechnol.*, 5, 1421 (**2005**).

176. F. Rohrbach, *CERN Report*, 71-5/TC-L, 19959.
177. A. v. Oostrom, *J. Appl. Phys*, 33, 2917 (**1962**).
178. R. Kurt, J. -M. Bonard, A. Karimi, *Thin Solid Films*, 98, 193 (**2001**).
179. R. Kurt, J. -M. Bonard, A. Karimi, *Carbon*, 39, 2163 (**2001**).
180. X. Ma, E.Wang, W. Zhou, D. Jefferson, J. Chen, S. Deng, N. Xu, J. Yuan, *Appl. Phys. Lett.*, 75, 3105 (**1999**).
181. P. Ding, E. Liang, M. Chao, X. Guo, *Physica E*, 25, 654 (**2005**).
182. D. Goldberg, P. S. Dorozhkin, Y. Bando, Z. –C. Dong, C. C. Tang, Y. Uemura, N. Grobert, M. Reyes-Reyes, H. Terrones, M. Terrones, *Appl. Phys. A*, 76, 499 (**2003**).
183. J. M. Bonard, R. Kurt, C. Klinke, *Chem. Phys. Lett.,* 343, 21 (**2001**).
184. G. Y. Zhang, X. C. Ma, D. Y. Zhong, E. G. Wang, *J. Appl. Phys*, 91, 9324 (**2002**).
185. J. –M. Bonhard, H. Kind, T. Stöckli, L.-O. Nilsson, *Sol. State Electron.*, 45, 893 (**2001**).
186. M. Doytecheva, M. Kaiser, M. A. Verheijen, M. Reyes-Reyes, M. Terrones, N. de Jonge, *Chem. Phys. Lett.*, 396, 126 (**2004**).
187. O. Groening, O. M. Kuettel, C. Emmenegger, P. Groening, L. Schlapbach, *J. Vac. Sci. Technol. B*, 18, 665 (**2000**).
188. G. Zhang, W. Duan, B. Gu, *Appl. Phys. Lett.*, 80, 2589 (**2002**).
189. S. Peng, K. Cho, *Nano Lett.*, 3, 513 (**2003**).
190. D. Y. Zhong, G. Y. Zhang, S. Liu, E. G. Wang, Q. Wang, H. Li, X. J. Huang, *Appl. Phys. Lett.*, 79, 3500 (**2001)**.
191. G. Maurin, F. Henn, ed. H. S. Nalwa *"Encyclopedia of Nanosciences and Nanotechnology. Vol. 2",* ASP, 773, (**2004**).
192. F. Hauke, A. Hirsch, *J. Chem. Soc. Chem. Commun.*, 21, 2199 (**1999**).
193. M. Terrones, N. Grobert, J. Olivares, J. P. Zhang, H. Terrones, K. Kordatos, W. K. Hsu, J.P. Hare, P. D. Townsend, K. Prassides, A. K. Cheetham, H. W. Kroto, D. R. M. Walton, *Nature*, 388, 52 (**1997**).
194. E. -G. Wang, *Adv. Mat.*, 11, 1129 (**1999**).
195. K. Suenaga, M. Yudasaka, C. Colliex, S. Iijima, *Chem. Phys. Lett.*, 316, 365 (**2000**).
196. X. B. Wang, W. P. Hu, Y. Q. Liu, C. F. Long, Y. Xu, S. Q. Zhou, D. Zhu, L. Dai, *Carbon*, 39, 1533 (**2001**).
197. Y. T. Lee, N. S. Kim, S. Y. Bae, J. Park, S. -C. Yu, H. Ryu, H. J. Lee, *J. Phys. Chem. B*, 107, 12958 (**2003**).
198. M. Terrones, R. Kamalakaran, T. Seeger, M. Rühle, *Chem. Comm.*, 23, 2335 (**2000**).
199. Z. Yang, Y. Xia, R. Mokaya, *Chem. Mater.*, 17, 4502 (**2005**).
200. S. Roche, F. Triozon, A. Rubio, D. Mayou, *Phys. Rev. B*, 64, 121401(R) (**2001**).
201. J. Robertson, C. A. Davis, *Diam. Rel. Mat*., 4, 441 (**1995**).